MAPPING OF THE ELECTRONIC STRUCTURE OF METALLOPROTEINS ONTO MULTI-ORBITAL ANDERSON MODEL USING THE DENSITY FUNCTIONAL THEORY

A Thesis Submitted to
the Graduate School of Engineering and Sciences of
İzmir Institute of Technology
in Partial Fulfillment of the Requirements for the Degree of

MASTER OF SCIENCE

in Physics

by
Zafer KANDEMİR

July 2013
İZMİR

We approve the thesis of **Zafer KANDEMİR**

Examining Committee Members:

Prof. Dr. Nejat BULUT
Department of Physics, Izmir Institute of Technology

Prof. Dr. Durmuş Ali DEMİR
Department of Physics, Izmir Institute of Technology

Prof. Dr. Nuran ELMACI
Department of Physics, Izmir Institute of Technology

10 July 2013

Prof. Dr. Nejat BULUT
Supervisor, Department of Physics
Izmir Institute of Technology

Prof. Dr. Nejat BULUT
Head of the Department of Physics

Prof. Dr. R. Tuğrul SENGER
Dean of the Graduate School of
Engineering and Sciences

ACKNOWLEDGMENTS

I would like to thank my supervisor Prof. Dr. Nejat Bulut for his great contribution. He has always been willing to listen to any problem and to provide helpful suggestions. I want to thank Prof. Dr. Ramazan Tuğrul Senger for his great contribution and helpful suggestions.

I would like to thank to the other members of my defence committee, Prof. Dr. Durmuş Ali Demir, Prof. Dr. Nuran Elmacı and Prof. Dr. Orhan Öztürk for helpful comments and giving suggestions.

I thank all my friends at İzmir Institute of Technology for their warm friendship and enjoyable times we spent. I also want to thank to Selma Mayda, Ozan Arı, Cihan Bacaksız, Mehmet Yağmurcukardeş, Jülide Yıldırım, Gözde Özbal, Fadıl İyikanat, Tuğrul Güner, Ayşe Elçiboğa, Canan Düztürk, Ozan Sargın and Duygu Şengün for their friendship and support.

Finally, I would like to thank my dear family for their endless support, encouragement, motivation and love during all my life.

ABSTRACT

MAPPING OF THE ELECTRONIC STRUCTURE OF METALLOPROTEINS ONTO MULTI-ORBITAL ANDERSON MODEL USING THE DENSITY FUNCTIONAL THEORY

In this thesis, an effective Haldane-Anderson model is constructed in order to describe the electronic properties of a system where a the transition-metal impurity atom is added into a semiconductor host material. Metalloenzymes and metalloproteins are proteins which contain a transition metal. Vitamin B_{12} is a metalloenzyme which contains a cobalt (Co) atom. The vitamin B_{12} exhibits semiconducting properties due to the presence of a semiconductor gap in the electronic density of states. Thus, we argue that the electronic properties of vitamin B_{12} can be studied within the framework of the Haldane-Anderson model. In this thesis, firstly, the electronic structure of vitamin B_{12}, which is known as cyanocobalamin, is obtained by using the Density Functional Theory (DFT) via the Gaussian program. By using the DFT results, the energies of the host and the $3d$ orbitals, and the hybridization terms between them are calculated. The final Haldane-Anderson Hamiltonian is obtained by adding the onsite Coulomb repulsion at the impurity $3d$ orbitals. The Haldane-Anderson Hamiltonian which has been constructed in this way from the DFT results can be studied by using the exact techniques many-body physics such as quantum Monte Carlo. Perturbative mean-field treats can also be used to study this Hamiltonian. Hence, the DFT calculations presented in this thesis represent the first step of thorough investigation of metalloproteins using these techniques of many-body physics.

ÖZET

YOĞUNLUK FONKSİYONELİ TEORİSİNİ KULLANARAK METALOPROTEİNLERİN ELEKTRONİK YAPISININ ÇOK YÖRÜNGELİ ANDERSON MODELİ ÇERÇEVESİNDE BETİMLENMESİ

Bu tezde, yarı-iletken ev sahibi malzemenin içine geçiş metali safsızlık atomu eklenmiş olan bir sistemin elektronik özelliklerini betimlemek için etkili bir Haldane-Anderson modeli oluşturulmuştur. Metaloenzimler ve metaloproteinler, içinde geçiş elementi bulunan proteinlerdir. Vitamin B_{12}, içinde kobalt atomu içeren metaloenzimdir. Vitamin B_{12}, durum yoğunluğu elektroniğinde bir yarı-iletken aralığının varlığından dolayı yarı-iletken özelliği gösterir. Böylece, vitamin B_{12}'nin elektronik özelliklerinin Haldane-Anderson modeli çerçevesinde çalışılabildiğini tartıştık. Bu tezde, ilk önce, Gaussian programı aracılığıyla Yoğunluk Fonksiyoneli Teorisini (YFT) kullanarak vitamin B_{12}'nin diğer bir adıyla cyanocobalamin'in elektronik yapısı elde edilmiştir. YFT sonuçları kullanılarak ev sahibi ve $3d$ yörüngelerinin enerjileri ve onlar arasındaki hibridizasyon terimleri hesaplanmıştır. Safsızlık $3d$ yörüngelerinde yerel Coulomb itmesi ekleyerek son Haldane-Anderson Hamiltonyen elde edilmiştir. YFT sonuçlarından oluşturulan Haldane-Anderson Hamiltonyen, kuantum Monte Carlo gibi çok parçacıklı fiziğin kesin teknikleri kullanarak çalışılabilinmektedir. Ayrıca, ortalama alan yaklaşımları bu Hamiltonyende kullanılabilir. Böylece, bu tezde sunulan YFT hesaplamaları çok parçacıklı fizik teknikleri kullanarak metaloproteinlerin ayrıntılı araştırılması ilk adımda gösterilmiştir.

TABLE OF CONTENTS

LIST OF FIGURES viii

LIST OF TABLES xii

CHAPTER 1. INTRODUCTION 1

CHAPTER 2. MAPPING OF ELECTRONIC STRUCTURE OF VITAMIN $\mathbf{B_{12}}$ ONTO THE ANDERSON MODEL 3

2.1. Background 3

2.2. Calculation of H_0 for the Host 5

2.3. Calculation of the Hybridization Term H_{hyb} 6

2.4. Second Quantized Form of the Hamiltonian 7

CHAPTER 3. DFT RESULTS AND DISCUSSIONS 10

3.1. NAO natural atomic orbitals 10

3.1.1. Why do we use the NAOs? 10

3.2. B3LYP for vitamin $\mathbf{B_{12}}$ from DFT with 6-31G(3d) basis set 17

3.2.1. Results 17

3.3. LSDA for vitamin $\mathbf{B_{12}}$ from DFT with 6-31G(3d) basis set 35

3.3.1. Results 36

CHAPTER 4. CONCLUSIONS 43

REFERENCES 46

APPENDICES

APPENDIX A. CALCULATION METHODS AND APPROXIMATIONS 52

APPENDIX B. HARTREE-FOCK MEAN FIELD APPROXIMATION FOR THE MULTI-ORBITAL ANDERSON MODEL 69

LIST OF FIGURES

Figure **Page**

Figure 3.1. Representation of the contributions of $3d$ orbitals by using nonorthogonal atomic orbitals (AOMO). 14
Figure 3.2. Representation of the energy values of $3d$ orbitals by using nonorthogonal atomic orbitals (AOMO). 15
Figure 3.3. Representation of the contributions of $3d$ orbitals by using orthogonal atomic orbitals (NAOMO). 16
Figure 3.4. Representation of the energy values of $3d$ orbitals by using orthogonal atomic orbitals (NAOMO). 17
Figure 3.5. Molecular structure of vitamin B_{12} (CNCbl = cyanocobalamin) with rings A-D, and the environment of corrin ring includes carbon atoms. Axially, the cobalt atom is coordinated on the lower face by a nitrogen from the intramolecular base 5,6-dimethylbenzimidazole (DMB) and on the upper face by cyano (CN). 22
Figure 3.6. Atomic position of cyanocobalamin, with the formidable empirical formula $\mathrm{C_{63}H_{88}CoN_{14}O_{14}P}$, (vitamin B_{12}). Nitrogen atoms are shown in dark blue, carbon in grey, cobalt in green, hydrogen in yellow, oxygen in red and phosphorus in orange. 23
Figure 3.7. In this figure, shown close to the atoms the environment of the cobalt atom. Here, in cyanocobalamin, the cobalt atom is surrounded by four nitrogen atoms in the corrin ring, it is bound to a nucleotide group and a CN group out of the corrin plane. 23
Figure 3.8. The Hamiltonian of the Fock matrix in the NAO basis (FNAO). We separated the Fock matrix into the three parts. The $\mathrm{H_d}$ part contains the diagonal terms $\varepsilon_{d\nu}$ (defining the effective energies of the $3d$ orbitals) and the off-diagonal terms $t_{\nu\nu'}$ (defining the hopping energies of the $3d$ orbitals). The H_0 matrix is represented the host Hamiltonian. The $\mathrm{M}_{\nu\mathrm{i}}$ and $\mathrm{M}_{\mathrm{i}\nu}$ parts include the interacting terms between the impurity (defining the $3d$ orbitals of cobalt atom) and the host part. 24
Figure 3.9. Energy eigenvalues E_n versus n for vitamin B_{12}. The forbidden energy gap (Δ) is approximately 2.71 eV between the HOMO and LUMO bands. Here, n is the number of basis functions; $n = 1, 2, \cdots, N$ 25

Figure 3.10. For all orbitals density of states $D(\varepsilon)$ versus ε are calculated by using Eq.(3.9). (a) The calculated density of state (DOS) of the vitamin B_{12} is plotted for $\gamma = 0.2$. (b) The x-axis is reduced in the range from -10 to 0 in order to demonstrate HOMO-LUMO region in much detail. This figure is broaden with ($\gamma = 0.1$). These plots are for 6-31G(3d) basis set. Here, the red solid line is the Fermi energy, at the same time, this line is the value of HOMO and also the red dashed line is the value of LUMO. In addition, these red lines are correspond to the values of HOMO and LUMO in the other figures. 26

Figure 3.11. The eigenvalues of host Hamiltonian ε_m versus m without $3d$ orbitals after diagonalization. The forbidden energy gap (Δ) is 2.59 eV between the HOMO and LUMO bands. Here, the value of m, which is the number of basis functions without the $3d$ orbitals, depends on the host part; $m = 1, 2, \cdots, N-5$ 27

Figure 3.12. Without $3d$ orbitals density of states $D_0(\varepsilon)$ versus ε are calculated by using Eq.(3.10). (a) The calculated density of state (DOS) without the $3d$ orbitals is plotted for $\gamma = 0.2$. The coloured vertical lines indicate the positions of the $3d$ orbitals. Here, the $3d$ orbitals are ordering $3z^2 - r^2$, xy, yz, $x^2 - y^2$, and xz, respectively. These orderings starts the highest occupancies of them. (b) The x-axis is reduced in the range from -10 to 0 in order to demonstrate HOMO-LUMO region in much detail. This figure is broaden with ($\gamma = 0.1$). These plots are for 6-31G(3d) basis set. 28

Figure 3.13. The host-impurity hybridization matrix elements $V_{\nu m}$ versus ε_m are calculated by using Eq.(3.11). (a) The hybridization matrix elements are shown between the host and $3z^2 - r^2$ orbital of cobalt atom. (b) The x-axis is reduced in the range from -10 to 0 in order to demonstrate HOMO-LUMO region in much detail. 29

Figure 3.14. The host-impurity hybridization matrix elements $V_{\nu m}$ versus ε_m are calculated by using Eq.(3.11). (a) The hybridization matrix elements between the host and xy orbital of cobalt atom. (b) The x-axis is reduced in the range from -10 to 0 in order to demonstrate HOMO-LUMO region in much detail. 30

Figure 3.15. The host-impurity hybridization matrix elements $V_{\nu m}$ versus ε_m are calculated by using Eq.(3.11). (a) The hybridization matrix elements between the host and yz orbital of cobalt atom. (b) The x-axis is reduced in the range from -10 to 0 in order to demonstrate HOMO-LUMO region in much detail. 31

Figure 3.16. The host-impurity hybridization matrix elements $V_{\nu m}$ versus ε_m are calculated by using Eq.(3.11). (a) The hybridization matrix elements between the host and $x^2 - y^2$ orbital of cobalt atom. (b) The x-axis is reduced in the range from -10 to 0 in order to demonstrate HOMO-LUMO region in much detail. 32

Figure 3.17. The host-impurity hybridization matrix elements $V_{\nu m}$ versus ε_m are calculated by using Eq.(3.11). (a) The hybridization matrix elements between the host and xz orbital of cobalt atom. (b) The x-axis is reduced in the range from -10 to 0 in order to demonstrate HOMO-LUMO region in much detail. 33

Figure 3.18. Constructed the new Hamiltonian H'. The first part contains the diagonal terms $\varepsilon_{d\nu}$ (defining the effective energies of the $3d$ orbitals) and the off-diagonal terms $t_{\nu\nu'}$ (defining the hopping energies of the $3d$ orbitals). The host part contains ε_m the eigenvalues of the host Hamiltonian after diagonalization. From Eq.(3.11), the $\mathrm{V}_{\nu\mathrm{m}}$ and $\mathrm{V}_{\mathrm{m}\nu}$ parts include the hybridization matrix elements between the impurity (defining the $3d$ orbitals of cobalt atom) and the host part. 34

Figure 3.19. Energy eigenvalues E_n versus n for vitamin B_{12}. The forbidden energy gap (Δ) is approximately 2.713 eV between the HOMO and LUMO bands. (a) The new eigenvalues of the H' denoted by the coloured blue is compared with the eigenvalues obtaining from Gaussian program indicated by the coloured black. (b) It is seen that these graphs are clearly the same each other. Here, the blue circle defines the eigenvalues of obtaining from Gaussian program and also the black triangle defines the eigenvalues of new Hamiltonian. 35

Figure 3.20. Energy eigenvalues E_n versus n for vitamin B_{12}. The forbidden energy gap (Δ) is approximately 1.93 eV between the HOMO and LUMO bands for alpha spin orbital. Here, n is the number of basis functions; $n = 1, 2, \cdots, N$ 40

Figure 3.21. For all orbitals density of states $D(\varepsilon)$ versus ε are calculated by using Eq.(3.17) for alpha spin orbital. (a) The calculated density of state (DOS) of the vitamin B_{12} is plotted for $\gamma = 0.2$. (b) The x-axis is reduced in the range from -10 to 0 in order to demonstrate HOMO-LUMO region in much detail. This figure is broaden with ($\gamma = 0.1$). These plots are for 6-31G(3d) basis set. Here, the red solid line is the Fermi energy, at the same time, this line is the value of HOMO and also the red dashed line is the value of LUMO. In addition, these red lines are correspond to the values of HOMO and LUMO in the other figures. . 41

Figure 3.22. Energy eigenvalues E_n versus n for vitamin B_{12}. The forbidden energy gap (Δ) is approximately 2.09 eV between the HOMO and LUMO bands for beta spin orbital. Here, n is the number of basis functions; $n = 1, 2, \cdots, N$ 42

Figure 3.23. For all orbitals density of states $D(\varepsilon)$ versus ε are calculated by using Eq.(3.17) for beta spin orbital. (a) The calculated density of state (DOS) of the vitamin B_{12} is plotted for $\gamma = 0.2$. (b) The x-axis is reduced in the range from -10 to 0 in order to demonstrate HOMO-LUMO region in much detail. This figure is broaden with ($\gamma = 0.1$). These plots are for 6-31G(3d) basis set. Here, the red solid line is the Fermi energy, at the same time, this line is the value of HOMO and also the red dashed line is the value of LUMO. In addition, these red lines are correspond to the values of HOMO and LUMO in the other figures. 43

LIST OF TABLES

Table **Page**

Table 3.1. The values of $t_{\nu\nu'}$ (off-diagonal terms) and $\varepsilon_{d\nu}$ (diagonal terms) of $3d$ orbitals in terms of eV. 19

Table 3.2. The values of occupancies and eigenvalues of the $3d$ orbitals. 20

Table 3.3. The values of $t_{\nu\nu'}$ (off-diagonal terms) and $\varepsilon_{d\nu}$ (diagonal terms) of $3d$ orbitals in terms of eV for the alpha spin orbital. 38

Table 3.4. The values of $t_{\nu\nu'}$ (off-diagonal terms) and $\varepsilon_{d\nu}$ (diagonal terms) of $3d$ orbitals in terms of eV for the beta spin orbital. 38

Table 3.5. The values of occupancies and eigenvalues of the $3d$ orbitals for the alpha spin orbital. 39

Table 3.6. The values of occupancies and eigenvalues of the $3d$ orbitals for the beta spin orbital. 39

Table 3.7. The values of magnetization is the difference between the occupancies of $3d$ orbitals for alpha spin and beta spin. 39

CHAPTER 1

INTRODUCTION

Proteins are the most important building blocks of organisms and they are absolutely essential in living organism for growth, development, repairing open wounds, digestion and synthesis of a variety of substances. Approximately one-third of all known proteins have a metal atom such as iron (Fe), cobalt (Co) and zinc (Zn), and also almost half of all enzymes require the presence of a metal atom to function. This metal is usually coordinated by nitrogen, oxygen or sulfur atoms. Such proteins and enzymes are named as metalloproteins and metalloenzymes that are organometallic molecules.

Metalloproteins [1–6] represent one of the most various classes of proteins in organometallic chemistry and metal in these molecules provides regulatory or structural roles to protein function. Metalloproteins have fascinated chemists and biochemists, particularly since the 1950s, when the first x-ray crystal structure of a protein, myoglobin, indicated the presence of an iron (Fe) atom. Examples of metalloproteins are hemoglobin and enzymes [3, 7–12]. They play important roles such as transfer of electron in life processes, cellular respiration, metabolism and immune system and also photosynthesis for plants, hemoglobin provides for transporting oxygen (O_2) and carbon dioxide (CO_2) gases to each living cells in a mammalian's body [13]. Example of metalloenzyme is vitamin B_{12} [4, 14–17]. It contains a cobalt (Co) atom as a transition metal impurity and involves in many important biological processes, including the normal functioning of the brain and nervous system and the formation of blood. It is involved in the metabolism of every cell of the body, especially affecting DNA synthesis and regulation [18].

Nowadays, many research groups have studied theoretically and experimentally metalloenzymes and metalloproteins in the areas of physics, biophysics, biochemistry and physical chemistry. For the study of molecular properties of these structures, computer software programs (Gaussian, Siesta, Quantum Espresso and Vasp) which are based on ab-initio methods are used. Physical and electronic structure calculations of these molecules are facilitated with developing these types of programs. The software of these programs have continuously been improved and updated. Now, many programs are able to do various calculations like energy by using density functional theory.

For the past four decades, density functional theory (DFT) has become very popular and successful method among quantum mechanical modelling theories which are used

in physics in order to examine the electronic structure of atoms, molecules and solids. An analytical solution of the many-body Schrödinger equation is not available for such complex systems. Hence, the DFT is widely used for the simulation of the energy surfaces in the complex molecules to overcome this problem and uses electron density formalism instead of wavefunction in order to describe the electronic structure of the systems.

Application of modern DFT calculations have been extended from small molecules to metal complexes in order to test the accuracy of the formalism. For complex molecules, DFT appears to be the method of choice at the moment. In the last few years, research groups have begun to apply DFT methods to a variety of systems such as metalloproteins, metalloenzymes, metalloporphyrins, biomolecules, polymers and macromolecules. Furthermore, to describe electronic properties of these structure, some models are used.

One of these models is Anderson model. The Anderson model was introduced by Anderson [21]. This model explains the magnetic properties of transition-metal impurities in semiconductors. The $3d$ orbitals of transition metals corresponds to the magnetic impurity part in the Anderson model, while the rest orbitals of the molecule can be considered as the host part of the Anderson model.

In this thesis, as an example of metalloenzymes, vitamin B_{12} is studied. The vitamin B_{12} is called cobalamin based on cobalt-containing compounds. The cobalamin comprise a R-ligand and a nucleotide attached to a corrin ring. The corrin ring is made up of four nitrogen atoms and an atom of cobalt in its center. The known vitamin B_{12} cofactors belong to (R-ligand) cobalamin (R-Cbl). Here the ligand is an ion, atom, or molecule that binds to a central metal atom. Vitamin B_{12} (cyanocobalamin, CNCbl) [19] is biologically inactive while the two cofactors are active as coenzymes B_{12} such as (R = adenosyl) adenosylcobalamin (AdoCbl) and (R = methyl) methylcobalamin (MeCbl) [3, 4, 14–16, 20].

Here, the electronic properties of vitamin B_{12} is studied by Anderson model. To construct the Anderson model Hamiltonian, we have used the density functional theory and calculated the impurity and the host energy levels as well as the hybridization matrix elements among these. However, the DFT is insufficient due to fact that the DFT does not take the contribution of onsite Coulomb interactions of $3d$ electrons into account. For this reason, the DFT does not give the correct electronic properties of systems. Consequently, we construct the multi-orbital Anderson model (for $U = 0$) to understand the magnetic semiconducting properties of vitamin B_{12}.

We investigate the energy and electronic structure of vitamin B_{12} that is known as cyanocobalamin (CNCbl) by using the density functional theory (DFT) via the Gaussian

program. Firstly, in Chapter 2, we represent the mapping of the electronic structure of the cyanocobalamin obtained from DFT onto the multi-orbital Anderson model. In Chapter 3, we calculate the molecular wavefunction and energy in detail by using the Becke3 (three parameters) Lee-Yang-Parr hybrid functional (B3LYP) and also we obtain the host band structure and the impurity-host hybridization matrix elements which are input parameters for the Haldane-Anderson model. In addition, we compute the molecular orbital and energy of vitamin B_{12} by using the local spin density approximation (LSDA) for spin polarized as alpha-spin and beta-spin orbitals. Finally, in Appendix A, the theoretical background of DFT is reviewed and in Appendix B, we explain Hartree-Fock mean field approximation for the multi-orbital Anderson model.

CHAPTER 2

MAPPING OF ELECTRONIC STRUCTURE OF VITAMIN $\mathrm{B_{12}}$ ONTO THE ANDERSON MODEL

2.1. Background

A density functional theory study of vitamin $\mathrm{B_{12}}$ which is also known as cyanocobalamin $(\mathrm{C_{63}H_{88}CoN_{14}O_{14}P})$, is carried out in order to determine the energy and the molecular wavefunctions. The wavefunctions, which are obtained from DFT calculations (See Appendix A) will be used to construct the Anderson Impurity Hamiltonian [21]. In cyanocobalamin, the cobalt atom which is surrounded by four nitrogen atoms in the corrin ring, and is bound to a nucleotide group and a CN group out of the corrin plane. The cobalt (Co) atom is described as the impurity atom in the Anderson model. By using the Gaussian 09 [22] within the DFT calculations, the molecular wavefunctions are obtained as a linear combination of Gaussian-type atomic orbitals.

Anderson model Hamiltonian was introduced by Anderson [21]. This Hamiltonian elucidates the magnetic properties of transition-metal impurities in semiconductors. Vitamin $\mathrm{B_{12}}$ exhibits magnetic semiconductor properties due to cobalt atom. The $3d$ orbitals of cobalt atom here corresponds to the magnetic impurity part in the Anderson model, while the rest orbitals of the molecule can be considered as the host part of the Anderson model. To construct the Anderson model Hamiltonian, we have used the density functional theory and calculated the impurity and the host energy levels as well as the hybridization matrix elements among these. However, the DFT is insufficient due to fact that the DFT does not take the contribution of onsite Coulomb interactions of $3d$ electrons into account. For this reason, the DFT does not give the correct electronic properties of systems. Consequently, we construct the multi-orbital Anderson model (for $U = 0$) to understand the magnetic semiconducting properties of vitamin $\mathrm{B_{12}}$.

In mapping to the Anderson model, we will dissociate the Hamiltonian into a part containing only the $3d$-orbitals of the cobalt atom, a part containing all the other orbitals except the $3d$ orbitals of Co, and finally a part which will describe the coupling of $3d$-orbitals of Co with the rest of atomic orbitals. Therefore, each molecular orbital will be

expressed as

$$|\psi_n\rangle = \sum_{\nu=1}^{5} \beta_{n\nu}|d_\nu\rangle + \sum_{i=1}^{N-5} \beta_{ni}|\phi_i\rangle \tag{2.1}$$

where β_{nm} are the molecular orbital coefficients, $|d_\nu\rangle$ is the orthogonal atomic orbital of impurity, and $|\phi_i\rangle$ is the orthogonal atomic orbital of host. In Eq.(2.1), n is an index for the molecular wavefunctions, N represents the number of the basis functions, the index ν refers to only $3d$ orbitals of cobalt atom and index i refers to the rest of the atomic orbitals (host index).

The single-particle Hamiltonian can be written as

$$H = \sum_{n=1}^{N} E_n |\psi_n\rangle\langle\psi_n| \, . \tag{2.2}$$

This Hamiltonian is expressed by using Eq.(2.1)

$$\begin{aligned} H = & \sum_{n=1}^{N} E_n \left(\sum_{i=1}^{N-5} \sum_{j=1}^{N-5} \beta_{ni}\beta_{nj}^* \right) |\phi_i\rangle\langle\phi_j| + \\ & + \sum_{n=1}^{N} E_n \left(\sum_{\nu=1}^{5} \sum_{i=1}^{N-5} \beta_{n\nu}\beta_{ni}^* |d_\nu\rangle\langle\phi_i| + h.c. \right) + \\ & + \sum_{\nu,\nu'=1}^{5} \left(\sum_{n=1}^{N} E_n \beta_{n\nu}\beta_{n\nu'}^* \right) |d_\nu\rangle\langle d_{\nu'}| \, . \end{aligned} \tag{2.3}$$

Thus, this Hamiltonian is classified into the following way

$$H = H_0 + H_{hyb} + H_{d0} \tag{2.4}$$

where

$$H_0 = \sum_{i,j=1}^{N-5} M_{ij}|\phi_i\rangle\langle\phi_j| \tag{2.5}$$

$$H_{hyb} = \sum_{\nu=1}^{5}\sum_{i=1}^{N-5} M_{\nu i}|d_\nu\rangle\langle\phi_i| + h.c. \tag{2.6}$$

$$H_{d0} = \sum_{\nu,\nu'=1}^{5} M_{\nu\nu'}|d_\nu\rangle\langle d_{\nu'}| \tag{2.7}$$

with

$$M_{\ell\ell'} = \sum_{n=1}^{N} E_n \beta_{n\ell}\beta^*_{n\ell'} \qquad \text{for} \quad 1 \leq \ell, \ell' \leq N. \tag{2.8}$$

Here H_0 represents the host Hamiltonian, H_{hyb} describes the hybridization between $3d$ orbitals and the host orbitals, and also H_{d0} represents the impurity Hamiltonian for the $3d$ orbitals. We also note that the natural bond orbitals (NBO) calculations are performed using NBO version 3.1 [23] which is attached to the Gaussian 09 program [22]. We can calculate molecular orbital coefficients both in the atomic orbital (AOMO) basis and in the orthogonal atomic orbital (NAOMO) basis thanks to the NBO program [23]. In Section 3.1, we will explain these relations in all details. The orthogonalities of the molecular orbitals denote in the NAO basis

$$\langle\psi_n|\psi_m\rangle = \delta_{nm} \quad \text{for NAOMO basis.} \tag{2.9}$$

Consequently, $|\phi_i\rangle$'s are given as an orthonormal basis set for NAOMO keyword.

2.2. Calculation of H_0 for the Host

From Eq.(2.3) and Eq.(2.5) with Eq.(2.8), H_0 becomes

$$H_0 = \sum_{i,j=1}^{N-5} M_{ij}|\phi_i\rangle\langle\phi_j| \tag{2.10}$$

which can be written as

$$H_0 = \sum_{i,j=1}^{N-5} h_{ij} |\phi_i\rangle\langle\phi_j| \ . \tag{2.11}$$

In the following step, we diagonalize $\underset{\sim}{h}$ matrix and obtain

$$H_0 = \sum_{m=1}^{N-5} \varepsilon_m |u_m\rangle\langle u_m| \tag{2.12}$$

where ε_m and $|u_m\rangle$ represent eigenvalues and eigenfunctions of the matrix $\underset{\sim}{h}$, and m describes the index of host orbitals.

2.3. Calculation of the Hybridization Term H_{hyb}

Any i'th column of the $\underset{\sim}{u}$ matrix is corresponding to i'th eigenvectors of the host Hamiltonian, where $i = 1, 2, \cdots, N-5$. The $\underset{\sim}{u}$ matrix elements are the coefficients of diagonalized eigenvectors on host atomic orbitals.

$$\underset{\sim}{u} = \begin{bmatrix} u_{11} & \cdots & u_{N-5,1} \\ u_{12} & \cdots & u_{N-5,1} \\ \vdots & \vdots & \vdots \\ u_{1,N-5} & \cdots & u_{N-5,N-5} \end{bmatrix}$$

In Section 2.2 for H_0, we have obtained $\underset{\sim}{u}$. Hence, $\left[\underset{\sim}{f}\right]_{(N-5)\times(N-5)}$ matrix is corresponding to $\underset{\sim}{f} = \underset{\sim}{u}$. Thus, H_{hyb} becomes

$$H_{hyb} = \sum_{\nu=1}^{5} \sum_{m=1}^{N-5} \left[\left(\sum_{i=1}^{N-5} M_{\nu i} f_{im} \right) |d_\nu\rangle\langle u_m| + h.c. \right] \ . \tag{2.13}$$

We next introduce $\underset{\sim}{V}$

$$V_{\nu m} \equiv \sum_{i=1}^{N-5} M_{\nu i} f_{im} \tag{2.14}$$

where $M_{\nu i}$ represents the hybridization part of the Fock matrix,

$$\left[\underset{\sim}{V}\right]_{5\times(N-5)} = \left[\underset{\sim}{M}\right]_{5\times(N-5)} \cdot \left[\underset{\sim}{f}\right]_{(N-5)\times(N-5)}$$

which defines the hybridization matrix elements between the impurity NAO's and the eigenstates of the host Hamiltonian. Thus, we obtain the hybridization term

$$H_{hyb} = \sum_{\nu=1}^{5}\sum_{m=1}^{N-5} \left(V_{\nu m}|d_\nu\rangle\langle u_m| + h.c.\right) \ . \tag{2.15}$$

2.4. Second Quantized Form of the Hamiltonian

The initial form of H is given by (from Eq.(2.4))

$$H = H_0 + H_{hyb} + H_{d0}$$

where

$$\begin{aligned} H_0 &= \sum_{i,j=1}^{N-5} M_{ij}|\phi_i\rangle\langle\phi_j| \\ H_{hyb} &= \sum_{\nu=1}^{5}\sum_{i=1}^{N-5} M_{\nu i}|d_\nu\rangle\langle\phi_i| + h.c. \\ H_{d0} &= \sum_{\nu,\nu'=1}^{5} M_{\nu\nu'}|d_\nu\rangle\langle d_{\nu'}| \ . \end{aligned}$$

In Section 2.2 , we have seen that H_0 can be written as

$$H_0 = \sum_{m=1}^{N-5} \varepsilon_m|u_m\rangle\langle u_m| \ . \tag{2.16}$$

Also from Section 2.3 we have

$$H_{hyb} = \sum_{\nu=1}^{5} \sum_{m=1}^{N-5} \left(V_{\nu m} |d_\nu\rangle\langle u_m| + h.c. \right) \ . \tag{2.17}$$

In addition, H_{d0} given by

$$H_{d0} = \sum_{\nu,\nu'=1}^{5} M_{\nu\nu'} |d_\nu\rangle\langle d_{\nu'}|$$

can be written as

$$H_{d0} = \sum_{\nu=1}^{5} \varepsilon_{d\nu} |d_\nu\rangle\langle d_\nu| + \sum_{\nu\neq\nu'}^{5} \left(t_{\nu\nu'} |d_\nu\rangle\langle d_{\nu'}| + h.c. \right) \ , \tag{2.18}$$

and

$$\varepsilon_{d\nu} = M_{\nu\nu} \ \text{, and} \ t_{\nu\nu'} = M_{\nu\nu'} \tag{2.19}$$

where $\varepsilon_{d\nu}$ defines the effective energies of the $3d$ orbitals and $t_{\nu\nu'}$ defines the hopping energies of the $3d$ orbitals.

From these results, we can obtain the second quantized form of the Hamiltonian as follows

$$H = H_0 + H_{hyb} + H_{d0}$$

where

$$H_0 = \sum_{\sigma} \sum_{m=1}^{N-5} \varepsilon_m c^{\dagger}_{m\sigma} c_{m\sigma} \tag{2.20}$$

$$H_{hyb} = \sum_{\sigma} \sum_{\nu=1}^{5} \sum_{m=1}^{N-5} \left(V_{\nu m} d^{\dagger}_{\nu\sigma} c_{m\sigma} + h.c. \right) \tag{2.21}$$

$$H_{d0} = \sum_{\sigma} \sum_{\nu=1}^{5} \varepsilon_{d_\nu} d^{\dagger}_{\nu\sigma} d_{\nu\sigma} + \sum_{\sigma} \sum_{\nu \neq \nu'}^{5} \left(t_{\nu\nu'} d^{\dagger}_{\nu\sigma} d_{\nu'\sigma} + h.c. \right). \tag{2.22}$$

After including the on-site Hubbard term for the d-orbitals, the final Anderson model Hamiltonian $\mathcal{H}$ is obtained

$$\mathcal{H} = H + H_U \tag{2.23}$$

where

$$H_U = \sum_{\nu} U_\nu n_{\nu\uparrow} n_{\nu\downarrow} \,. \tag{2.24}$$

We note that in this form of the Hamiltonian, H_0 describes the electronic states without including the cobalt $3d$ orbitals.

We also note that H_{d0} has an effective hopping term between the $3d$ orbitals. Hence, the part of the Hamiltonian which only contains the $3d$ orbitals, $H_{d0} + H_U$, can be considered as an effective 5-site Hubbard model. In this perspective, the total Hamiltonian $\mathcal{H}$ can be considered as a 5-site Hubbard model embedded into an effective host described by H_0.

CHAPTER 3

DFT RESULTS AND DISCUSSIONS

3.1. NAO natural atomic orbitals

The analysis of natural atomic orbital (NAO) and natural bond orbital (NBO) have been developed by Weinhold and coworkers to define the shape of atomic orbitals in the molecule, and to derive molecular bonds from electron density between atoms [24]. In this article, according to NAO procedure, nonorthogonal AOs $\{\phi_i\}$ are transformed to corresponding orthogonal AOs $\{\tilde{\phi}_i\}$ by the occupancy-weighted symmetric orthogonalization (OWSO) procedure

$$T_{OWSO}\{\phi_i\} = \{\tilde{\phi}_i\} \ , \ \langle\tilde{\phi}_i|\tilde{\phi}_j\rangle = \delta_{ij} \tag{3.1}$$

Here, the transformation matrix T_{OWSO} has the mathematical property of minimizing the occupancy-weighted, and has the mean-squared deviations of the nonorthogonal ϕ_i and the orthogonal $\tilde{\phi}_i$

$$min\Big\{\sum_i w_i \int |\tilde{\phi}_i - \phi_i|^2 d\tau\Big\}. \tag{3.2}$$

where weighting factor w_i is defined as

$$w_i = \langle\phi_i|\hat{\Gamma}|\phi_i\rangle. \tag{3.3}$$

Eq.(3.3) is taken as the occupancy of nonorthogonal ϕ_i and $\hat{\Gamma}$ is defined as diagonal expectation value of the density operator.

3.1.1. Why do we use the NAOs?

In our first calculation, we use the molecular orbital coefficients that are given by Gaussian program. These molecular orbital coefficients are given in terms of atomic

orbitals

$$\langle \psi_n | \psi_m \rangle \neq \delta_{nm} \quad \text{for AOMO basis.} \tag{3.4}$$

The accuracy of orthogonality has been proved by using overlap matrix. Then, we try to obtain the energy values of $3d$ orbitals with the following equation

$$\varepsilon_{d\nu}(N) = \sum_{n=1}^{N} E_n |\beta_{n\nu}|^2. \tag{3.5}$$

Here, the value of N is the number of basis functions. Due to high coefficients we has found high energy values with Eq.(3.5) have been seen above zero. In addition, in Fig.(3.1), we plot the absolute squared of $3d$ orbital coefficients $|\beta_{n\nu}|^2$ with the energy eigenvalues of molecular orbitals E_n. In Fig.(3.1), each figures show the contributions of $3d$ orbitals. We are worried about the contributions which have been seen above zero for each figures. These results does not make sense to us. Then, we start to use the following equation.

$$\varepsilon_{d\nu}(M) = \frac{\sum_{n=1}^{M} E_n |\beta_{n\nu}|^2}{\sum_{n=1}^{M} |\beta_{n\nu}|^2} \tag{3.6}$$

In Eq.(3.6), the value of M is changing from 1 to the number of basis function N. We find large and unreasonable results again. Therefore, after we plot relation between $\varepsilon_{d\nu}(M)$ and ε_M in Fig.(3.2), we estimate the value of M. The specific results are achieved with the value of M, but to verify these results, we make the literature review. After that, we found orthogonal atomic orbitals with NAOMO and orbitals of energies with FNAO by using NBO program which is attached to the Gaussian program. For NAOMO basis, we prove the accuracy of orthogonality as follows

$$\langle \psi_n | \psi_m \rangle = \delta_{nm} \quad \text{for NAOMO basis.} \tag{3.7}$$

NBO program defines the various keywords to obtain coefficients and energy values. We obtain the energy values of $3d$ orbitals from the following equation by using orthogonal

atomic orbital coefficients $\beta_{n\nu}$ and energy eigenvalues E_n.

$$\varepsilon_{d\nu} = \sum_{n=1}^{N} E_n |\beta_{n\nu}|^2. \tag{3.8}$$

In addition, in Fig.(3.3), we plot the relation between $|\beta_{n\nu}|^2$ and E_n by using orthogonal atomic orbital coefficients. There is no contributions to the last part in each figure. In Fig.(3.4), we plot the relation between $\varepsilon_{d\nu}(M)$ and ε_M by using orthogonal atomic orbital coefficients. The contributions of the last part are remained constant. Moreover, we obtain directly energy values $\varepsilon_{d\nu}$ and hopping energy values $t_{\nu\nu'}$ of $3d$ orbitals from Fock matrix. The energy values of $3d$ orbitals which are calculated Eq.(3.8) and elements of Fock matrix are same. Therefore, we continue our calculation by using Fock matrix.

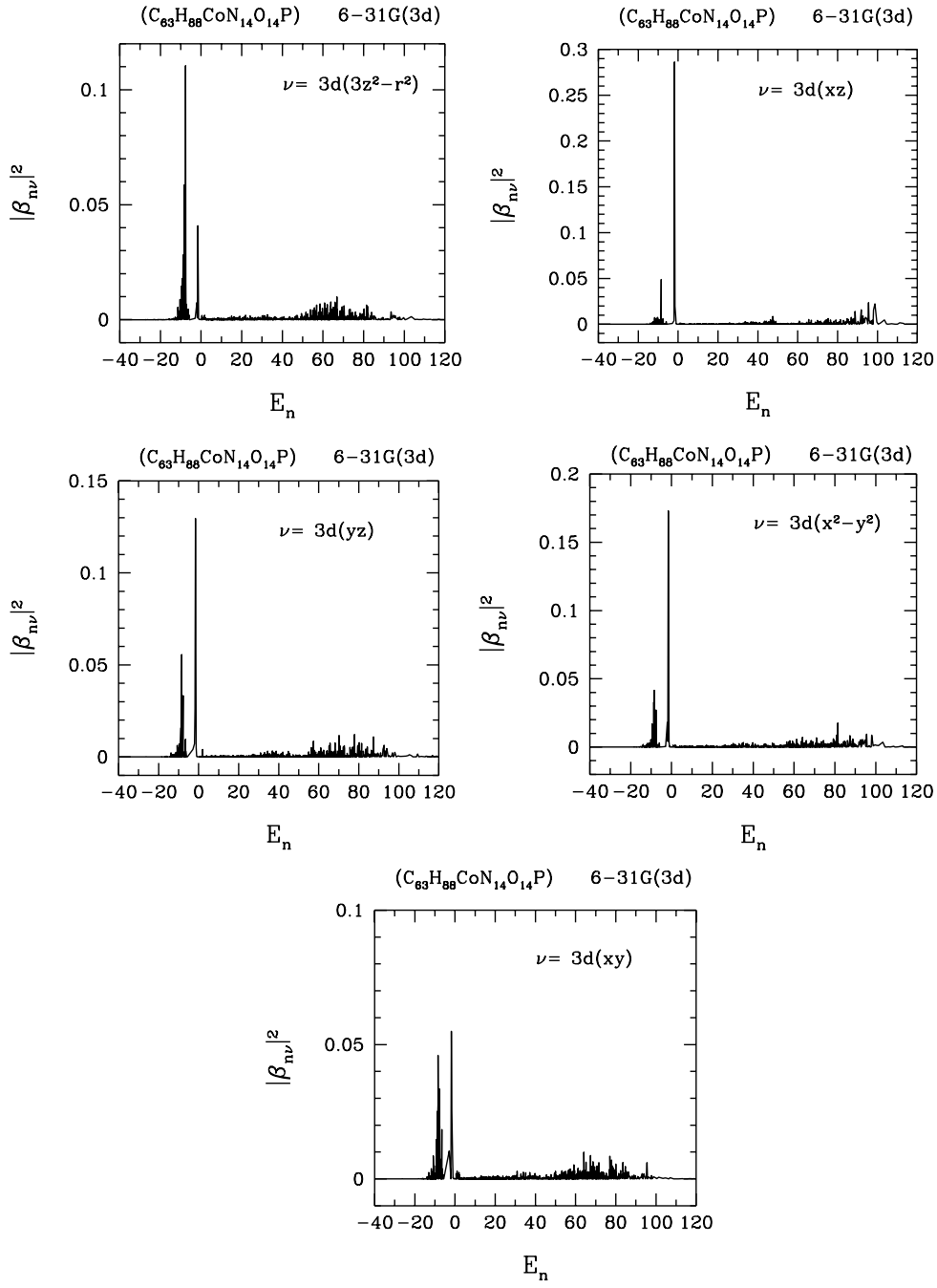

Figure 3.1. Representation of the contributions of $3d$ orbitals by using nonorthogonal atomic orbitals (AOMO).

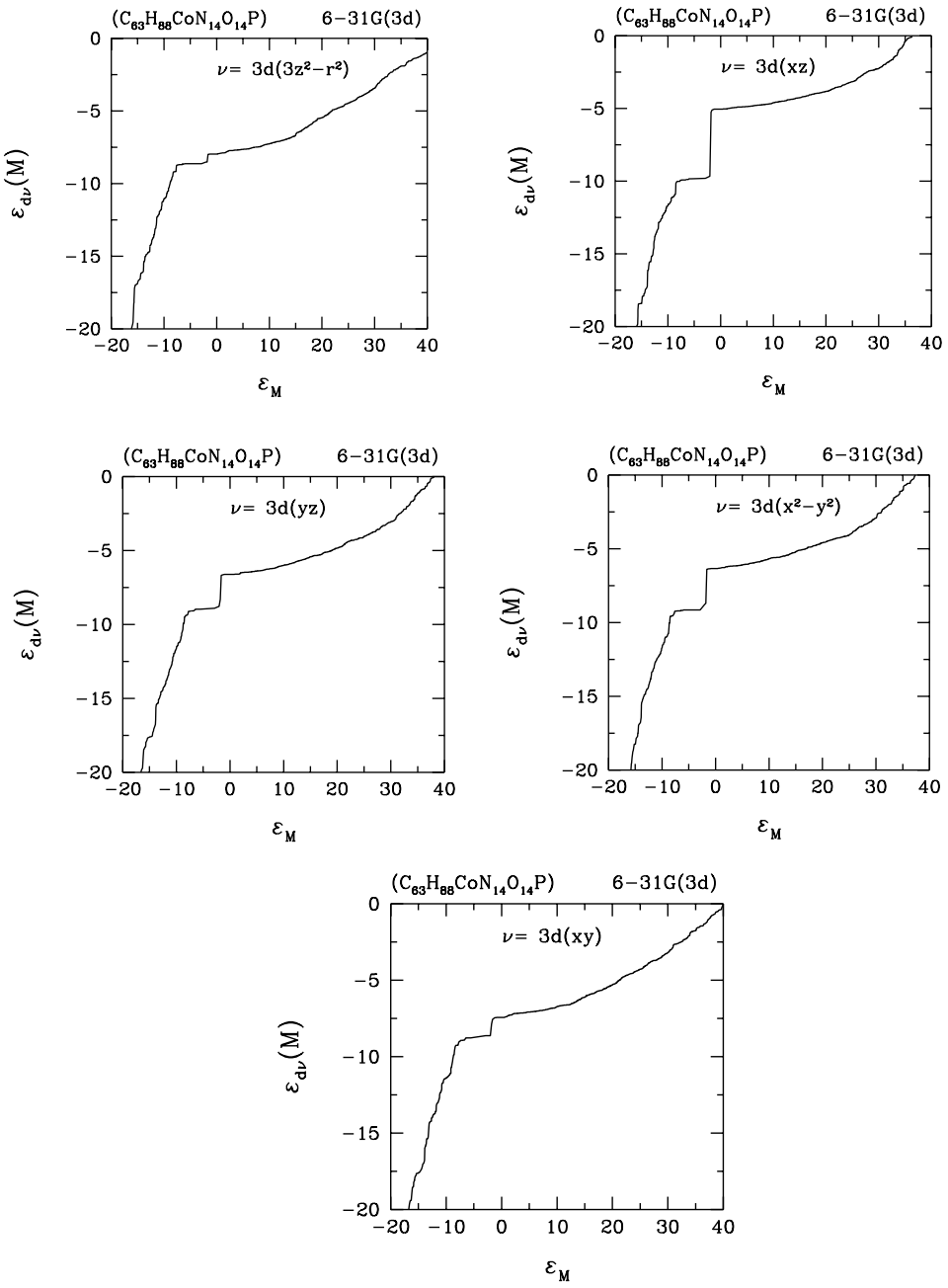

Figure 3.2. Representation of the energy values of $3d$ orbitals by using nonorthogonal atomic orbitals (AOMO).

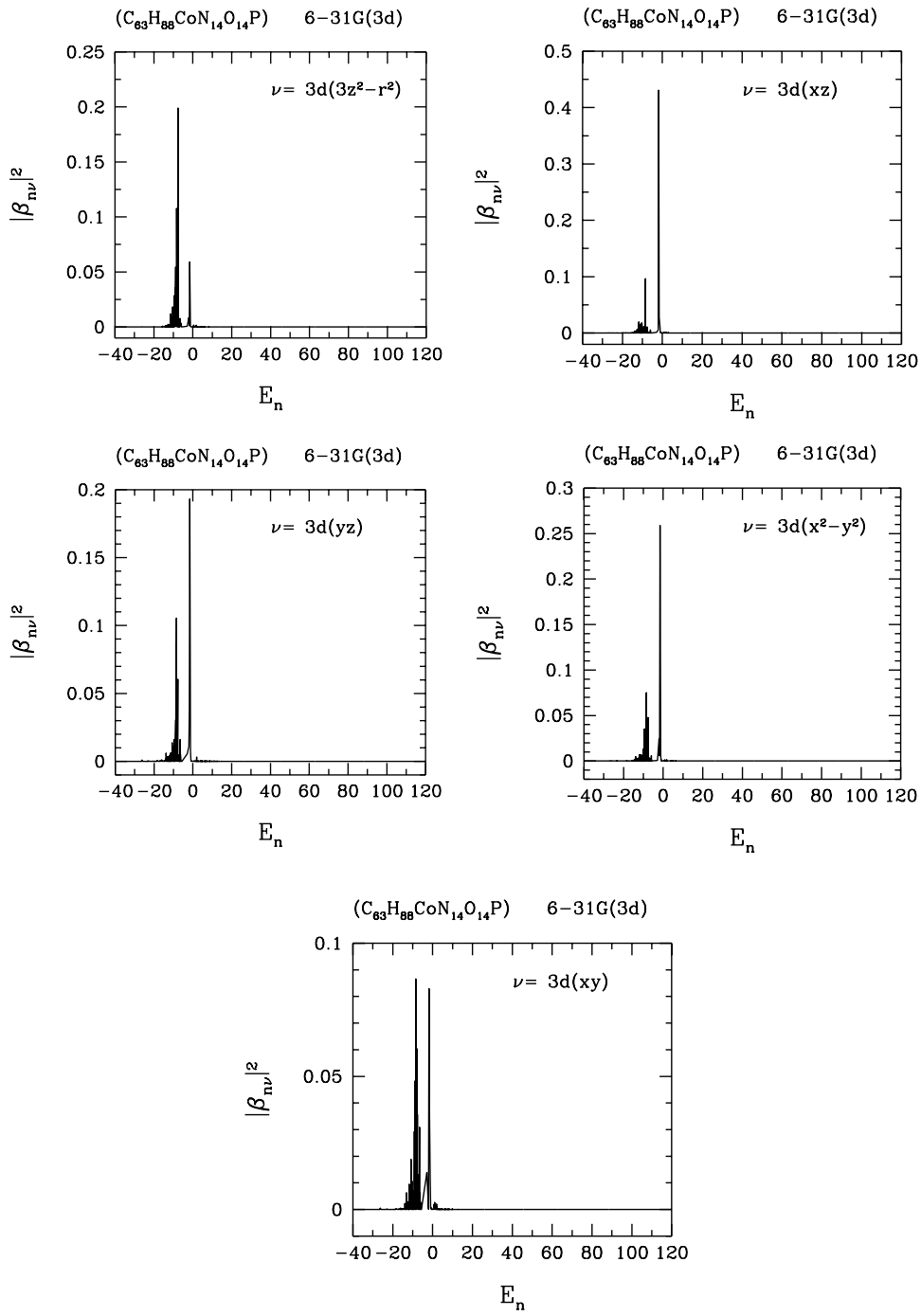

Figure 3.3. Representation of the contributions of $3d$ orbitals by using orthogonal atomic orbitals (NAOMO).

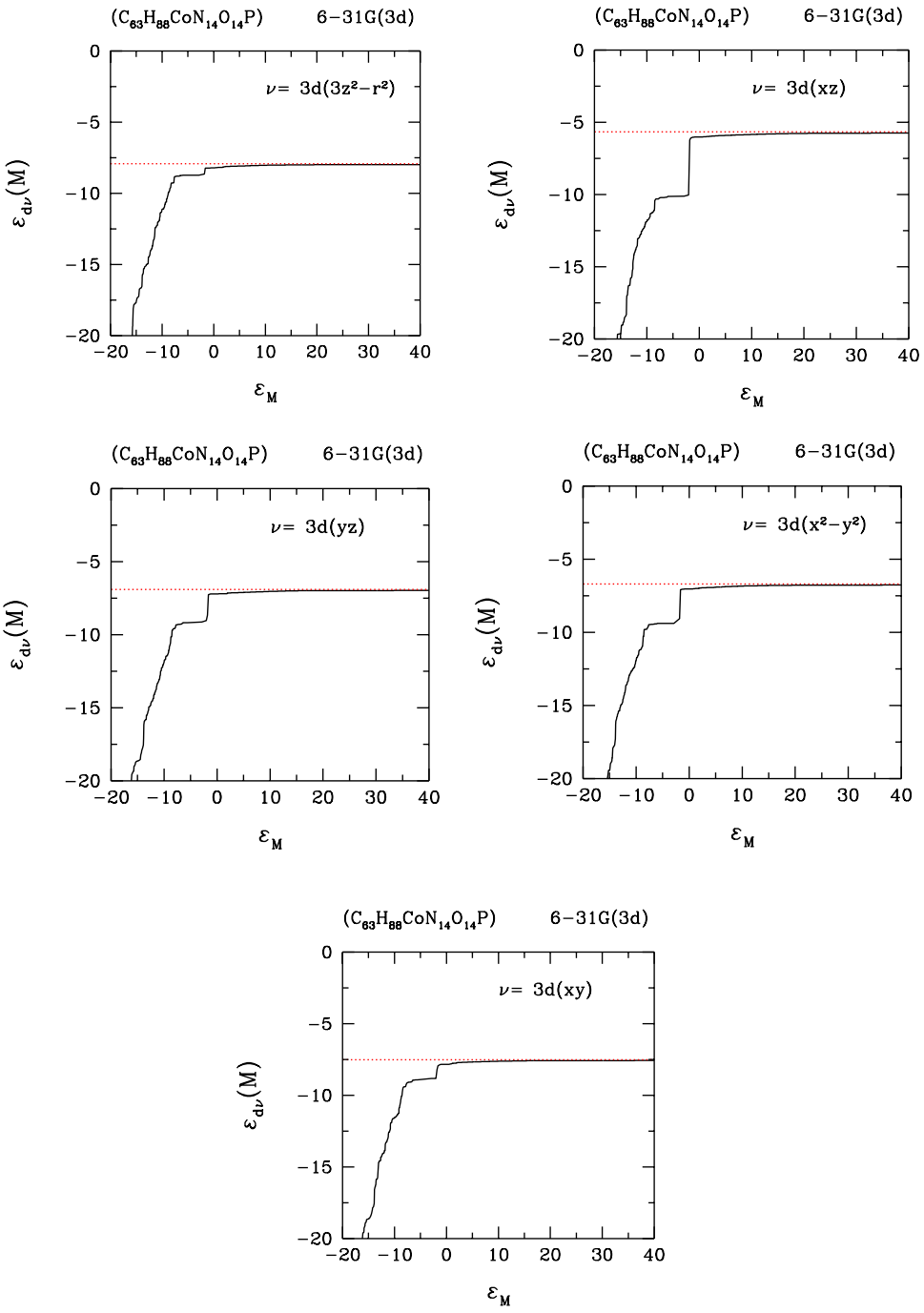

Figure 3.4. Representation of the energy values of $3d$ orbitals by using orthogonal atomic orbitals (NAOMO).

3.2. B3LYP for vitamin B_{12} from DFT with 6-31G(3d) basis set

We have obtained the electronic structure of the vitamin B_{12} (cyanocobalamin) by using the Density Functional Theory (DFT) via the Gaussian program [22]. Molecular geometry is obtained by using GaussView [25] molecular visualization program and Gaussian 09 program [22] package on our server. In this calculation, the cyanocobalamin has been optimized by using the DFT at the hybrid functional B3LYP level with LANL2DZ basis set for Co atom and 6-31G(3d) basis set for the rest of the atoms (C, H, O, N, P). For the transition metal Co atom, the effective core potential basis set LANL2DZ (Los Alamos ECP plus double zeta) is used for its valence electrons and core electrons are treated with LANL2 effective core potential [26, 27]. The cyanocobalamin is the most complex tetrapyrrolic cofactor in which the central cobalt atom is coordinated by four equatorial nitrogen ligands donated by pyrroles A-D of the corrin ring [4, 28]. The molecular structure of cyanocobalamin is shown in Fig.(3.5) [4, 15, 16, 19, 29–35], for the atomic positions via GaussView [25] in Figs.(3.6 and 3.7).

When the keyword "pop=NBORead" is written the Gaussian input file, we can calculate the coefficients for molecular orbitals (MO) in terms of atomic orbitals (AOMO), natural atomic orbitals (NAOMO) and also the elements of Fock matrix in terms of the atomic orbitals (FAO) basis and the natural atomic orbitals (FNAO) basis. We note that the natural atomic orbitals refer to orthogonal atomic orbitals. The natural bonding orbitals (NBO) calculations are performed by using NBO version 3.1 [23] which is attached to the Gaussian 09 [22]. An useful aspect of the NBO method is that it gives information about interaction in both occupied and virtual spaces. The NBO analysis provides an efficient method for studying intra and inter-molecular bonding and interaction among bonds [36]. We obtain the Fock matrix in terms of orthogonal atomic orbitals (FNAO) by using NBO program. The FNAO is significant parameter for our investigation. In addition, we acquire the occupancies of the $3d$ orbitals. These quantities are derived from the NBO population analysis.

3.2.1. Results

When we obtain the Fock matrix in the NAO basis, in Fig.(3.8), we can divide our Hamiltonian into sub-matrices which is denoted host Hamiltonian and coupling part of $3d$ orbitals . The host Hamiltonian H_0 is the interacting part between the host and the $3d$

orbitals. The coupling part of $3d$ orbitals directly gives the effective energies $\varepsilon_{d\nu}$ (diagonal terms) of the $3d$ orbitals of cobalt atom and the hopping energies $t_{\nu\nu'}$ (off-diagonal terms) of the $3d$ orbitals of cobalt atom.

In Fig.(3.9), the energy eigenvalues E_n versus the eigenstate index n are shown by using Gaussian output file. Here we see that the forbidden energy gap (Δ) is 2.71 eV which is the difference of the highest occupied molecular orbital (HOMO) and the lowest unoccupied molecular orbital (LUMO) energies. We also note that the number of basis functions is $N = 2436$ for 6-31G(3d) basis set.

Fig.(3.10) shows the density of states (DOS) defined by

$$\begin{aligned} D(\varepsilon) &= \sum_{n=1}^{N} \delta(\varepsilon - E_n) \\ &= \sum_{n=1}^{N} \frac{\gamma/\pi}{\gamma^2 + (\varepsilon - E_n)^2} \end{aligned} \tag{3.9}$$

versus ε . The Fermi level (ε_{F}) is indicated by the red solid line at -5.57 eV.

In Table 3.1, we show the values of $t_{\nu\nu'}$ (off-diagonal terms) and $\varepsilon_{d\nu}$ (diagonal terms) in eV. We obtain this table thanks to the Fock matrix in the orthogonal atomic orbitals (FNAO).

Table 3.1. The values of $t_{\nu\nu'}$ (off-diagonal terms) and $\varepsilon_{d\nu}$ (diagonal terms) of $3d$ orbitals in terms of eV.

eV	$3z^2$-r^2	xy	yz	x^2-y^2	xz
$3z^2$-r^2	-7.92668	0.32382	-0.59049	0.59049	0.12245
xy	0.32382	-7.51035	-0.77552	0.51702	-0.92519
yz	-0.59049	-0.77552	-6.90081	-1.27077	0.40817
x^2-y^2	0.59049	0.51702	-1.27077	-6.68856	0.66124
xz	0.12245	-0.92519	0.40817	0.66124	-5.65181

In Table 3.2, we show the values of occupancies of the $3d$ orbitals. We obtain these values from the natural population analysis.

After the host Hamiltonian is diagonalized, we obtain the energy eigenvalues ε_m of the host part without the $3d$ orbitals. The energies are represented in Fig.(3.11) as a function of corresponding eigenstate indices.

Table 3.2. The values of occupancies and eigenvalues of the $3d$ orbitals.

3d orbitals	ε_d (eV)	$\langle n_\nu \rangle$
$3z^2$-r^2	-7.92668	1.81975
xy	-7.51035	1.65561
yz	-6.90081	1.44569
x^2-y^2	-6.68856	1.36078
xz	-5.65181	0.98964

In Fig.(3.12), we demonstrate that the positions of $3d$ orbitals are added in the density of state (DOS). The DOS is defined by

$$\begin{aligned} D_0(\varepsilon) &= \sum_{m=1}^{N-5} \delta(\varepsilon - \varepsilon_m) \\ &= \sum_{m=1}^{N-5} \frac{\gamma/\pi}{\gamma^2 + (\varepsilon - \varepsilon_m)^2} \ . \end{aligned} \tag{3.10}$$

It is clear from this figure that the $3d$ orbitals are located near the HOMO-LUMO energy gap.

When we divide the Fock matrix, we obtain the eigenvalues ε_m and eigenvectors u_m of the host Hamiltonian after diagonalization. In Section 2.3, we obtain the hybridization matrix elements by using

$$V_{\nu m} = \sum_{i}^{N-5} M_{\nu i} f_{im} \ . \tag{3.11}$$

In Figs.(3.13, 3.14, 3.15, 3.16, 3.17), we represent the hybridization matrix elements between the host and the $3d$ orbitals of the cobalt atom. From here, we construct the new Hamiltonian H' in Fig.(3.18) in order to check our calculations. Then, after we diagonalize the new Hamiltonian, we obtain its new eigenvalues and eigenvectors. In Fig.(3.19), it is seen that the new eigenvalues of H' are equal to the eigenvalues which are obtained by Gaussian program.

Finally, we obtain the Fermi level of this system as -5.57 eV, the eigenvalues of the host part ε_m, and the effective energy of the $3d$ orbitals $\varepsilon_{d\nu}$ by using the Fock

matrix, and also obtain the impurity-host hybridization matrix elements which are the input parameters for the Haldane-Anderson model.

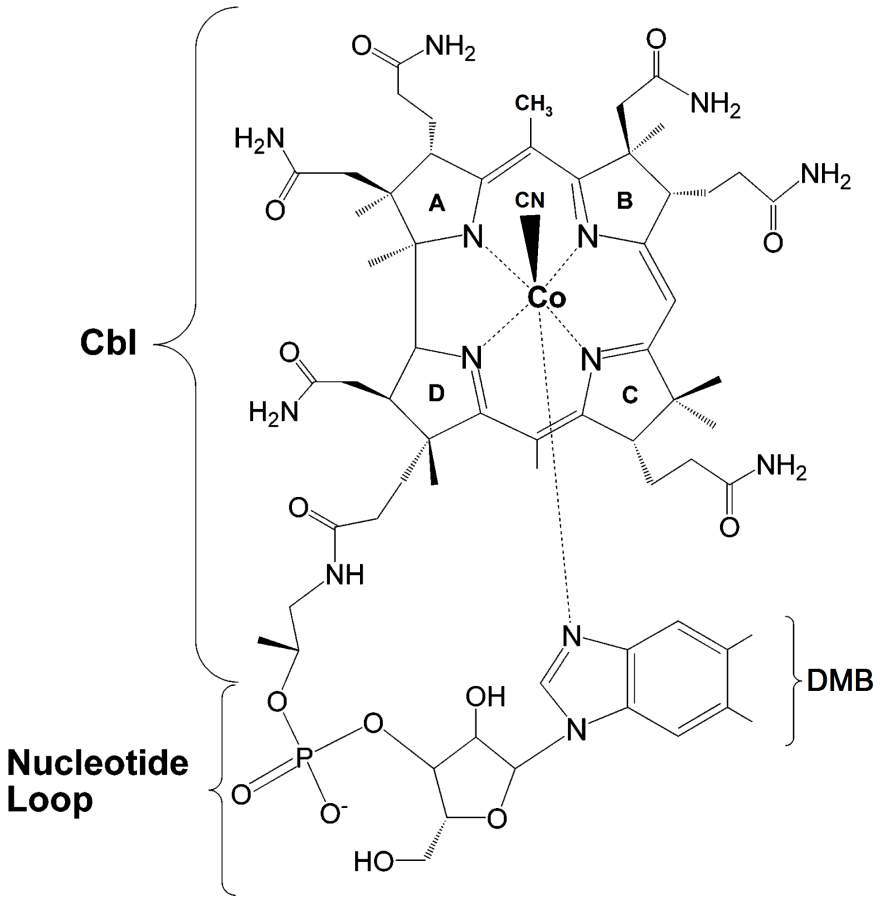

Figure 3.5. Molecular structure of vitamin B_{12} (CNCbl = cyanocobalamin) with rings A-D, and the environment of corrin ring includes carbon atoms. Axially, the cobalt atom is coordinated on the lower face by a nitrogen from the intramolecular base 5,6-dimethylbenzimidazole (DMB) and on the upper face by cyano (CN).

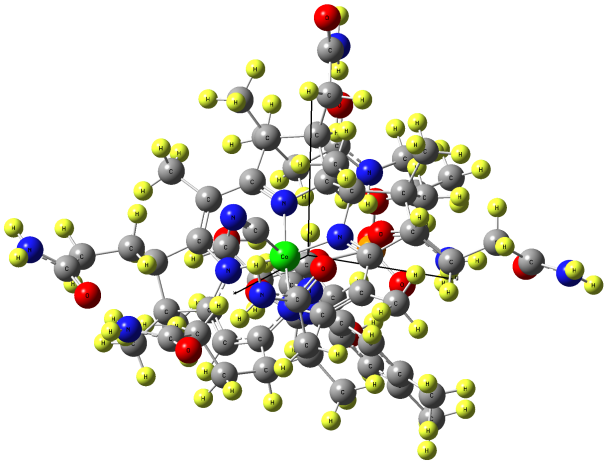

Figure 3.6. Atomic position of cyanocobalamin, with the formidable empirical formula $C_{63}H_{88}CoN_{14}O_{14}P$, (vitamin B_{12}). Nitrogen atoms are shown in dark blue, carbon in grey, cobalt in green, hydrogen in yellow, oxygen in red and phosphorus in orange.

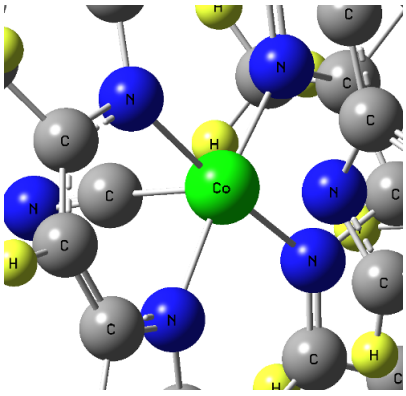

Figure 3.7. In this figure, shown close to the atoms the environment of the cobalt atom. Here, in cyanocobalamin, the cobalt atom is surrounded by four nitrogen atoms in the corrin ring, it is bound to a nucleotide group and a CN group out of the corrin plane.

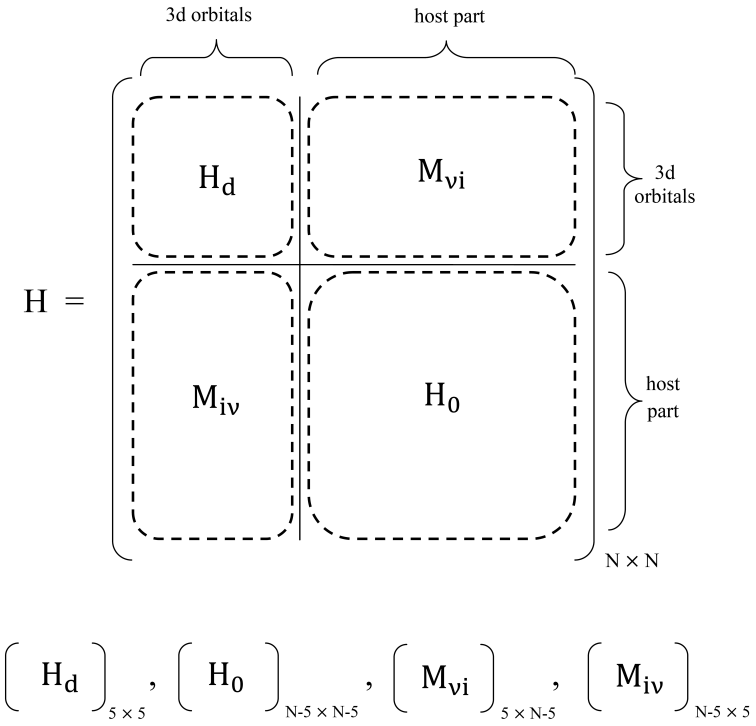

Figure 3.8. The Hamiltonian of the Fock matrix in the NAO basis (FNAO). We separated the Fock matrix into the three parts. The $\mathrm{H_d}$ part contains the diagonal terms $\varepsilon_{d\nu}$ (defining the effective energies of the $3d$ orbitals) and the off-diagonal terms $t_{\nu\nu'}$ (defining the hopping energies of the $3d$ orbitals). The $\mathrm{H_0}$ matrix is represented the host Hamiltonian. The $\mathrm{M_{\nu i}}$ and $\mathrm{M_{i\nu}}$ parts include the interacting terms between the impurity (defining the $3d$ orbitals of cobalt atom) and the host part.

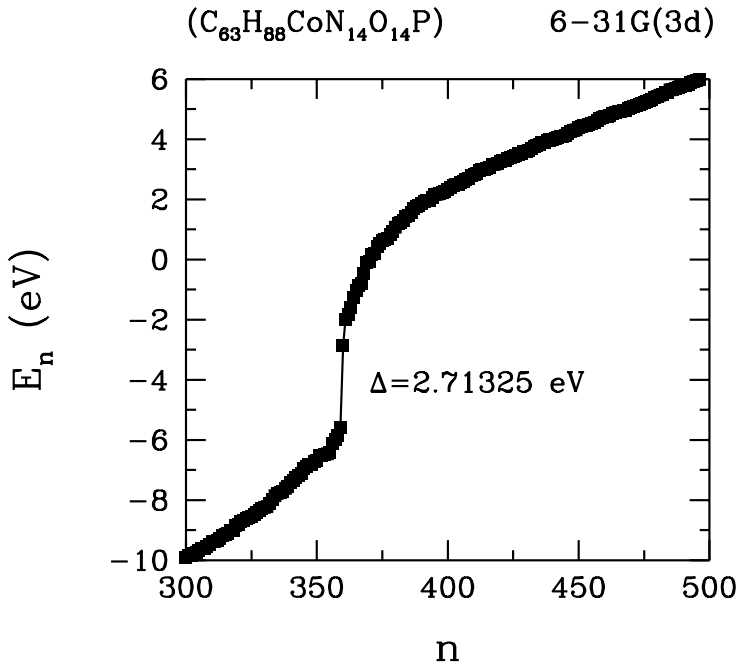

Figure 3.9. Energy eigenvalues E_n versus n for vitamin B_{12}. The forbidden energy gap (Δ) is approximately 2.71 eV between the HOMO and LUMO bands. Here, n is the number of basis functions; $n = 1, 2, \cdots, N$.

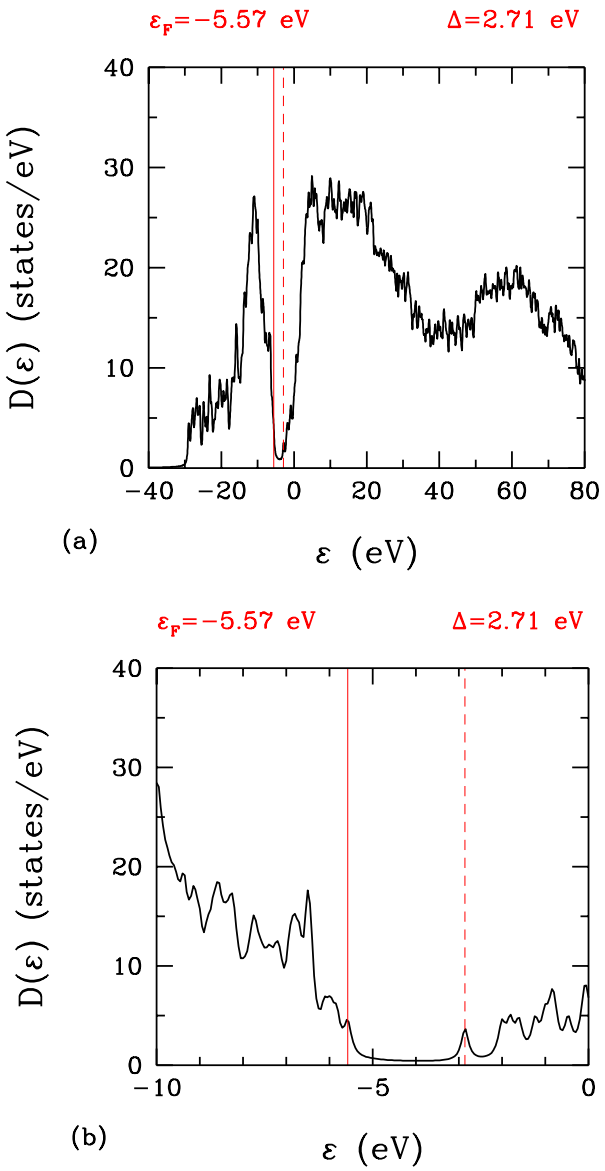

Figure 3.10. For all orbitals density of states $D(\varepsilon)$ versus ε are calculated by using Eq.(3.9). (a) The calculated density of state (DOS) of the vitamin B_{12} is plotted for $\gamma = 0.2$. (b) The x-axis is reduced in the range from -10 to 0 in order to demonstrate HOMO-LUMO region in much detail. This figure is broaden with ($\gamma = 0.1$). These plots are for 6-31G(3d) basis set. Here, the red solid line is the Fermi energy, at the same time, this line is the value of HOMO and also the red dashed line is the value of LUMO. In addition, these red lines are correspond to the values of HOMO and LUMO in the other figures.

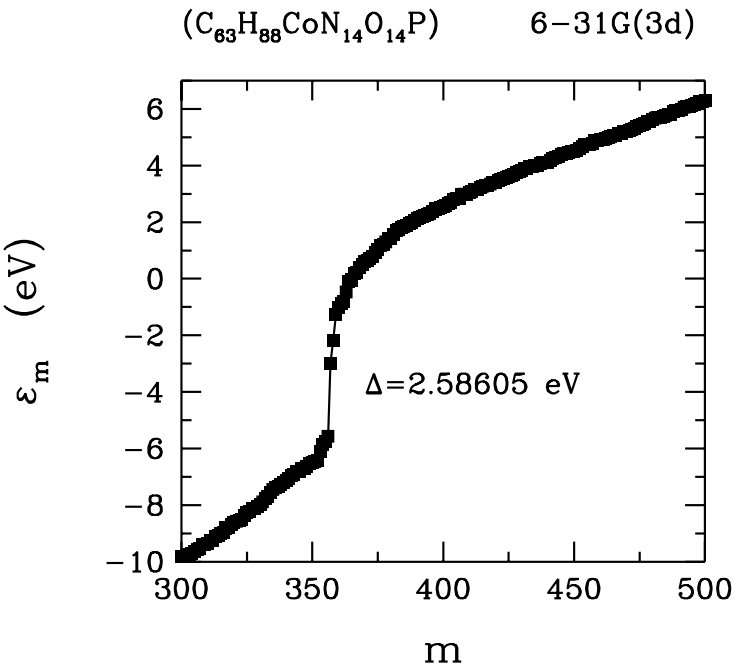

Figure 3.11. The eigenvalues of host Hamiltonian ε_m versus m without $3d$ orbitals after diagonalization. The forbidden energy gap (Δ) is 2.59 eV between the HOMO and LUMO bands. Here, the value of m, which is the number of basis functions without the $3d$ orbitals, depends on the host part; $m = 1, 2, \cdots, N-5$.

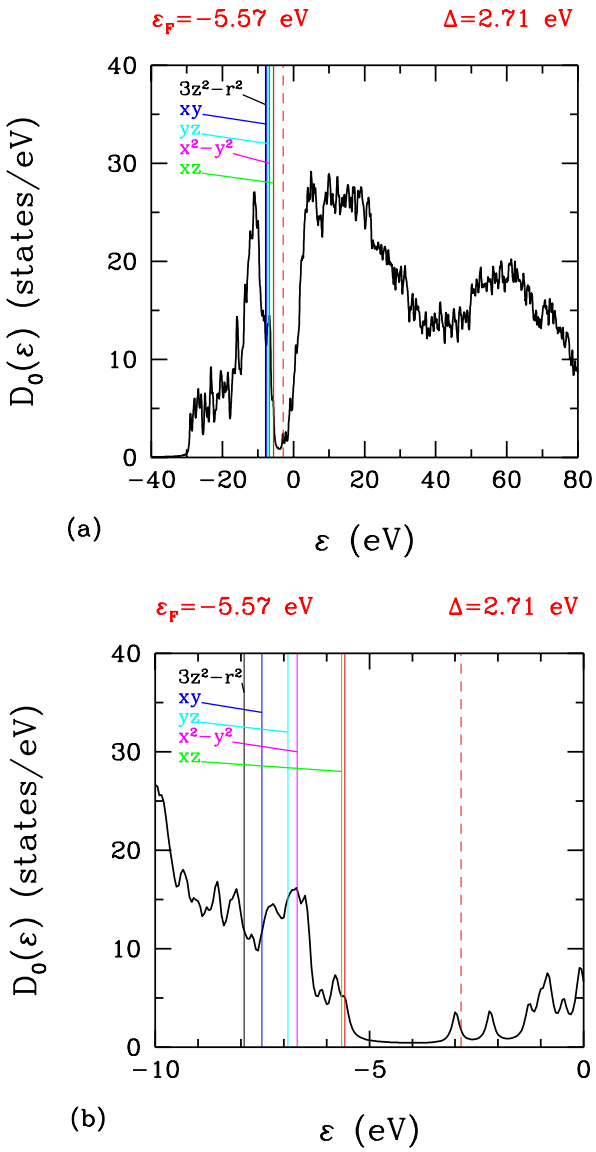

Figure 3.12. Without $3d$ orbitals density of states $D_0(\varepsilon)$ versus ε are calculated by using Eq.(3.10). (a) The calculated density of state (DOS) without the $3d$ orbitals is plotted for $\gamma = 0.2$. The coloured vertical lines indicate the positions of the $3d$ orbitals. Here, the $3d$ orbitals are ordering $3z^2 - r^2$, xy, yz, $x^2 - y^2$, and xz, respectively. These orderings starts the highest occupancies of them. (b) The x-axis is reduced in the range from -10 to 0 in order to demonstrate HOMO-LUMO region in much detail. This figure is broaden with ($\gamma = 0.1$). These plots are for 6-31G(3d) basis set.

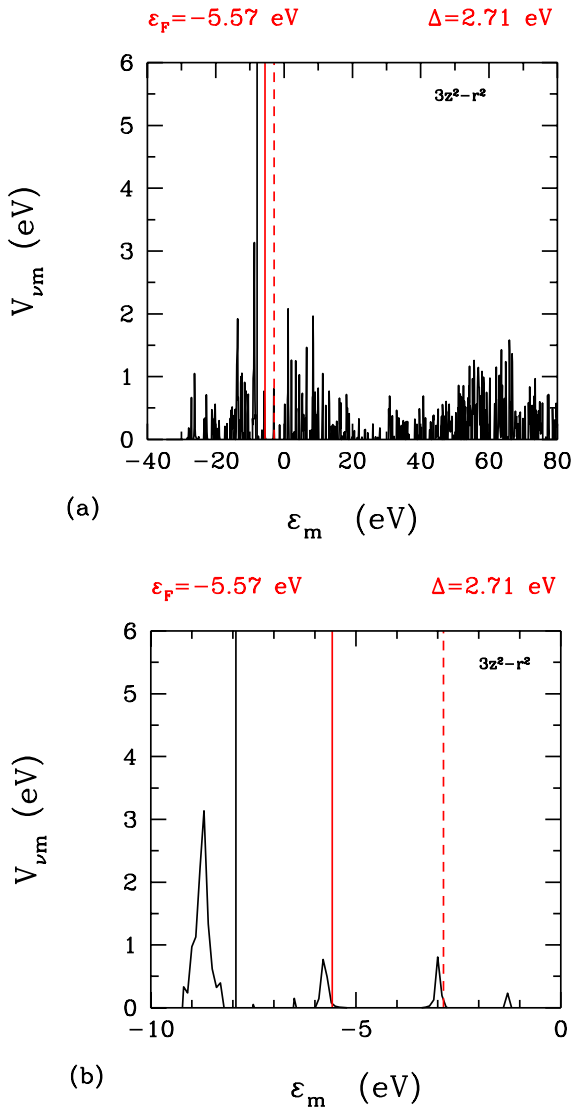

Figure 3.13. The host-impurity hybridization matrix elements $V_{\nu m}$ versus ε_m are calculated by using Eq.(3.11). (a) The hybridization matrix elements are shown between the host and $3z^2 - r^2$ orbital of cobalt atom. (b) The x-axis is reduced in the range from -10 to 0 in order to demonstrate HOMO-LUMO region in much detail.

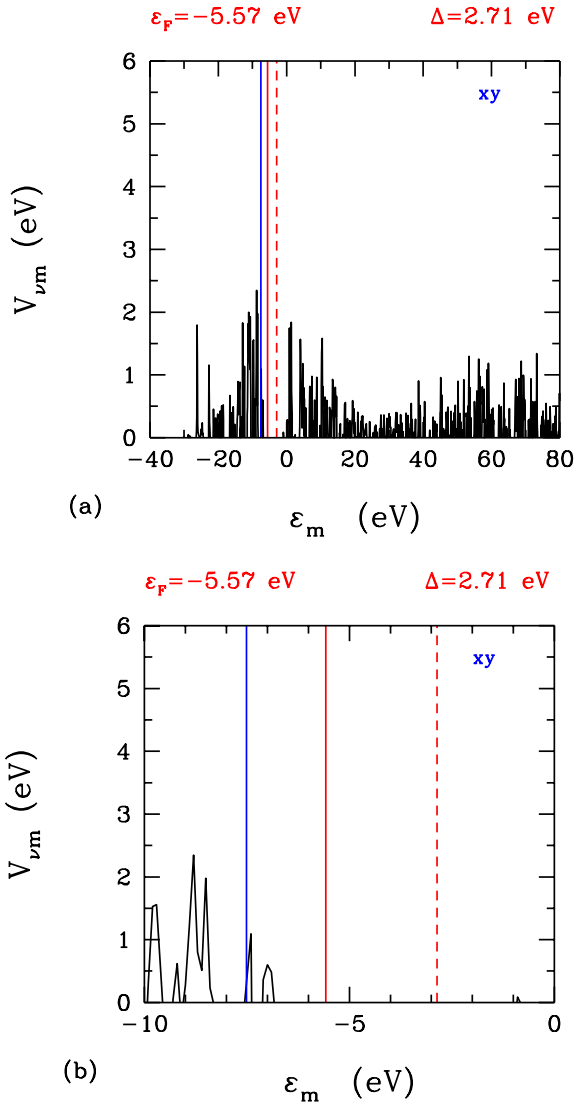

Figure 3.14. The host-impurity hybridization matrix elements $V_{\nu m}$ versus ε_m are calculated by using Eq.(3.11). (a) The hybridization matrix elements between the host and xy orbital of cobalt atom. (b) The x-axis is reduced in the range from -10 to 0 in order to demonstrate HOMO-LUMO region in much detail.

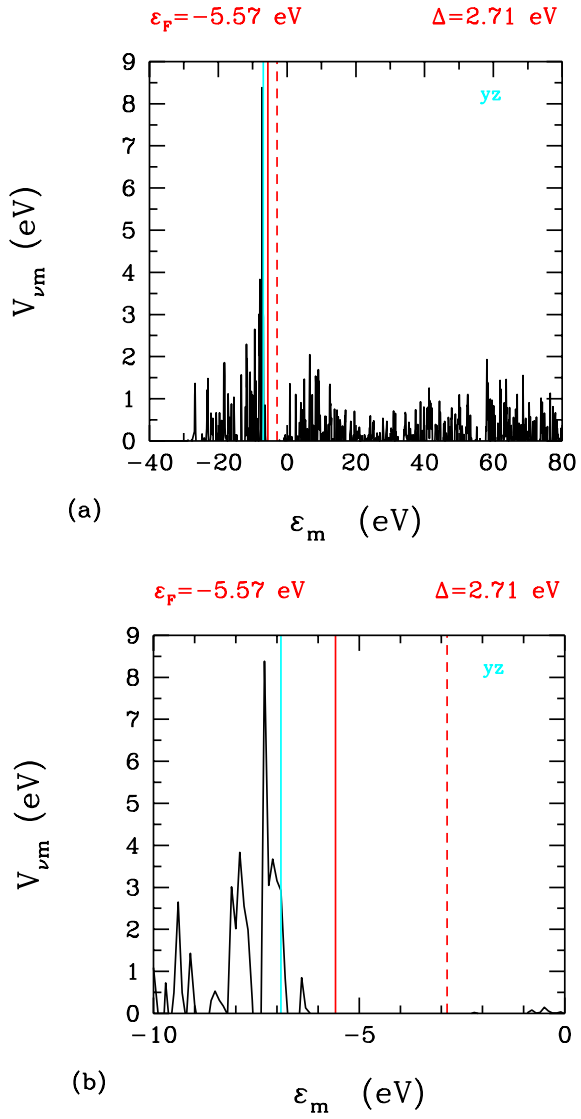

Figure 3.15. The host-impurity hybridization matrix elements $V_{\nu m}$ versus ε_m are calculated by using Eq.(3.11). (a) The hybridization matrix elements between the host and yz orbital of cobalt atom. (b) The x-axis is reduced in the range from -10 to 0 in order to demonstrate HOMO-LUMO region in much detail.

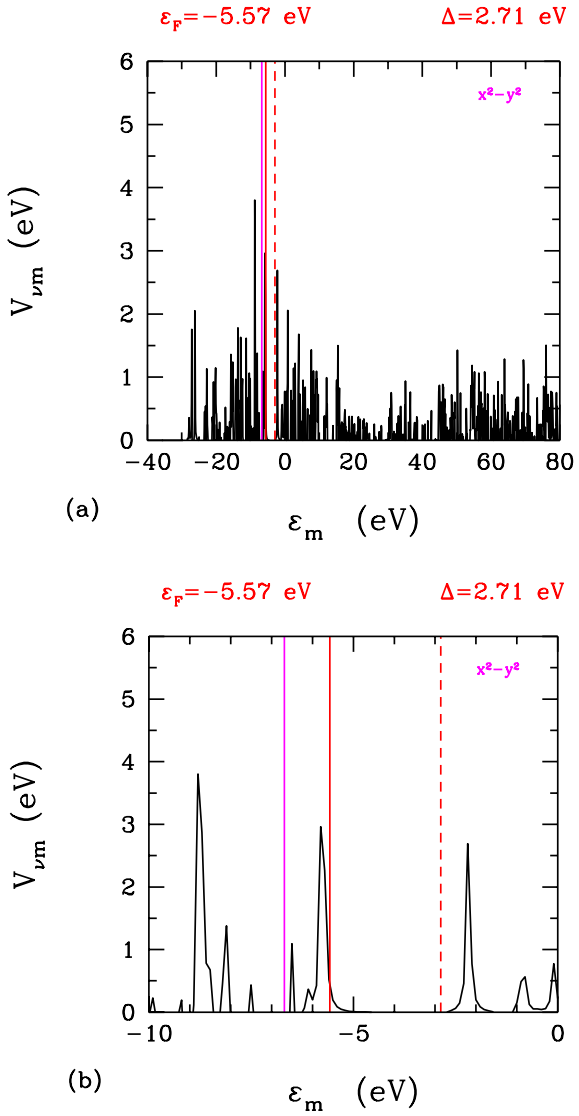

Figure 3.16. The host-impurity hybridization matrix elements $V_{\nu m}$ versus ε_m are calculated by using Eq.(3.11). (a) The hybridization matrix elements between the host and $x^2 - y^2$ orbital of cobalt atom. (b) The x-axis is reduced in the range from -10 to 0 in order to demonstrate HOMO-LUMO region in much detail.

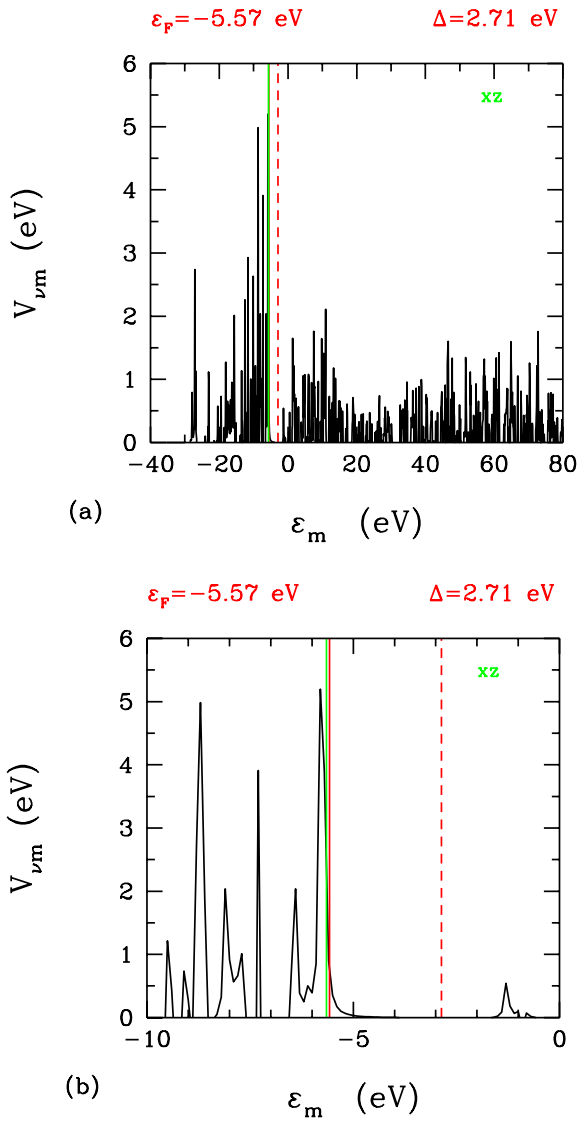

Figure 3.17. The host-impurity hybridization matrix elements $V_{\nu m}$ versus ε_m are calculated by using Eq.(3.11). (a) The hybridization matrix elements between the host and xz orbital of cobalt atom. (b) The x-axis is reduced in the range from -10 to 0 in order to demonstrate HOMO-LUMO region in much detail.

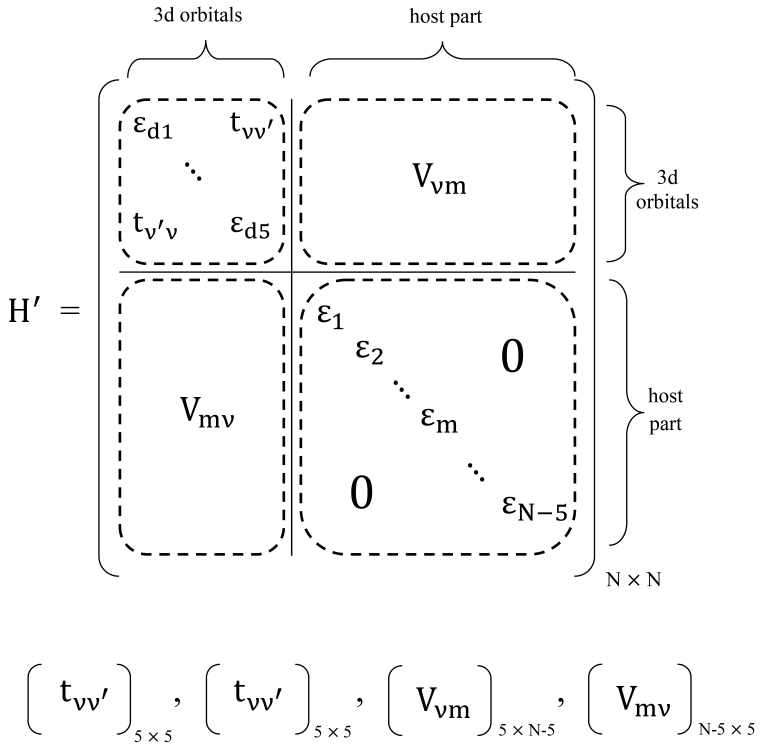

Figure 3.18. Constructed the new Hamiltonian H'. The first part contains the diagonal terms $\varepsilon_{d\nu}$ (defining the effective energies of the $3d$ orbitals) and the off-diagonal terms $t_{\nu\nu'}$ (defining the hopping energies of the $3d$ orbitals). The host part contains ε_m the eigenvalues of the host Hamiltonian after diagonalization. From Eq.(3.11), the $\mathrm{V}_{\nu\mathrm{m}}$ and $\mathrm{V}_{\mathrm{m}\nu}$ parts include the hybridization matrix elements between the impurity (defining the $3d$ orbitals of cobalt atom) and the host part.

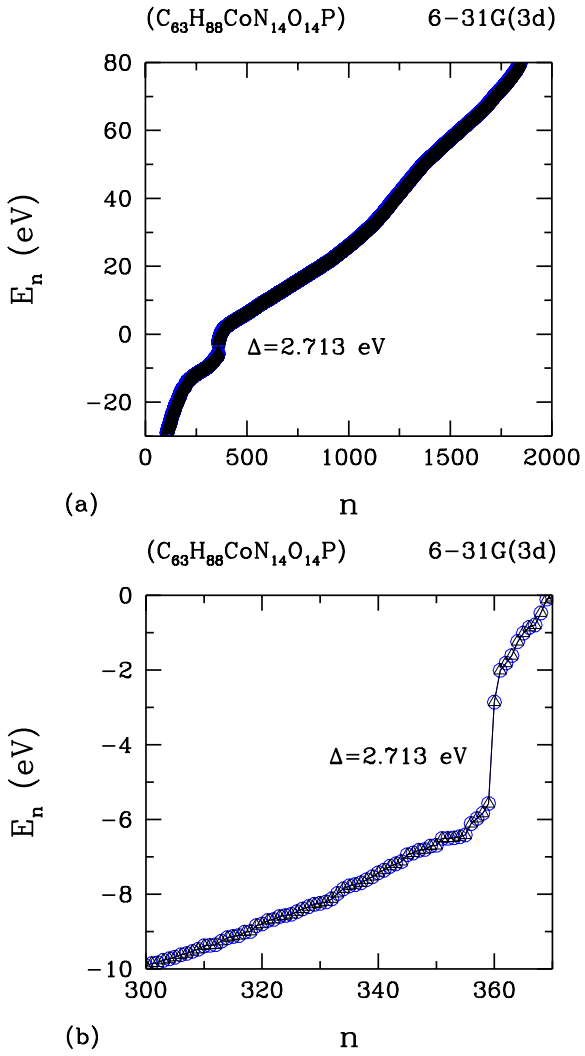

Figure 3.19. Energy eigenvalues E_n versus n for vitamin B_{12}. The forbidden energy gap (Δ) is approximately 2.713 eV between the HOMO and LUMO bands. (a) The new eigenvalues of the H' denoted by the coloured blue is compared with the eigenvalues obtaining from Gaussian program indicated by the coloured black. (b) It is seen that these graphs are clearly the same each other. Here, the blue circle defines the eigenvalues of obtaining from Gaussian program and also the black triangle defines the eigenvalues of new Hamiltonian.

3.3. LSDA for vitamin B_{12} from DFT with 6-31G(3d) basis set

For open-shell molecules and molecular geometries near dissociation, the local spin density approximation (LSDA) gives better outcomes than the local density approximation (LDA) (See Appendix A). Whereas in the LDA, electrons with the opposite spins paired with each other have the same atomic orbital [37]. The LSDA allows such electrons to have different spatial atomic orbitals ψ_i^α and ψ_i^β. Thus, in LSDA, one deals separately with the electron density $\rho_\alpha(\boldsymbol{r})$ due to spin-up electrons and density $\rho_\beta(\boldsymbol{r})$ owing to spin-down electrons.

In LSDA, the exchange-correlation functional energy (for spin-polarized systems) is defined by

$$E_{xc}^{LSDA}[\rho_\alpha, \rho_\beta] = E_x^{LSDA}[\rho_\alpha, \rho_\beta] + E_c^{LSDA}[\rho_\alpha, \rho_\beta]. \tag{3.12}$$

The LSDA exchange energy is

$$E_x^{LSDA}[\rho_\alpha, \rho_\beta] = \int \rho(\boldsymbol{r})\epsilon_x(\rho, \xi)d\boldsymbol{r} \tag{3.13}$$

where

$$\epsilon_x(\rho, \xi) = \epsilon_x^P(\rho) + \left[\epsilon_x^F(\rho) - \epsilon_c^P(\rho)\right] \frac{1}{2}\left(\frac{(1+\xi)^{4/3} + (1-\xi)^{4/3} - 2}{2^{1/3} - 1}\right) \tag{3.14}$$

with $\epsilon_x^P = \epsilon_x(\rho_\alpha = \rho_\beta = \frac{\rho}{2})$ for the paramagnetic (non-polarized) and $\epsilon_x^F = \epsilon_x(\rho_\alpha = \rho\ ,\ \rho_\beta = 0)$ for the ferromagnetic (completely spin-polarized) limits of the functional and ξ is the relative spin polarization

$$\xi = \frac{\rho_\alpha - \rho_\beta}{\rho_\alpha + \rho_\beta}. \tag{3.15}$$

The LSDA correlation energy is

$$E_c^{LSDA}[\rho_\alpha, \rho_\beta] = \int \rho(\boldsymbol{r})\epsilon_c(r_s, \xi)d\boldsymbol{r}. \tag{3.16}$$

The $\epsilon_c(r_s, \xi)$ is fitted to the ground state energy of a homogeneous electron gas calculated using quantum Monte Carlo simulations and similar spin-interpolations. There is no analytical function for uniform electron gas.

In this calculation, the cyanocobalamin has been calculated by using the DFT at

the LSDA with LANL2DZ basis set for Co atom and 6-31G(3d) basis set for the other atoms. When the keywords "pop=NBORead" and "FNAO" are supplemented our Gaussian input file, we obtain the Fock matrix in terms of orthogonal atomic orbitals (FNAO) by using NBO program.

3.3.1. Results

In this section, the Fock matrix and the electron numbers of $3d$ orbitals are obtained from LSDA method. Especially, in LSDA, the alpha-spin orbital and the beta-spin orbital are divided into two parts. Thus, we obtain separately the Fock matrix for alpha and beta spin orbitals.

After obtaining the Fock matrix for alpha and beta spin orbitals, in Fig.(3.8), we can divide our Hamiltonian into sub-matrices which is denoted host Hamiltonian and coupling part of $3d$ orbitals . The host Hamiltonian H_0 is the interacting part between the host and the $3d$ orbitals. The coupling part of $3d$ orbitals directly gives the effective energies $\varepsilon_{d\nu}$ (diagonal terms) of the $3d$ orbitals of cobalt atom and the hopping energies $t_{\nu\nu'}$ (off-diagonal terms) of the $3d$ orbitals of cobalt atom.

In Figs.(3.20 and 3.22), the energy eigenvalues E_n versus the eigenstate index n are shown by using Gaussian output file for each spin orbitals. Here we see that the forbidden energy gap is the difference of the highest occupied molecular orbital (HOMO) and the lowest unoccupied molecular orbital (LUMO) energies.

Figs.(3.21 and 3.23) shows the density of states (DOS) defined by

$$\begin{aligned} D(\varepsilon) &= \sum_{n=1}^{N} \delta(\varepsilon - E_n) \\ &= \sum_{n=1}^{N} \frac{\gamma/\pi}{\gamma^2 + (\varepsilon - E_n)^2} \end{aligned} \tag{3.17}$$

versus ε for each spin orbitals. The Fermi level (ε_F) is shown by the red solid line at -5.72 eV for the alpha spin orbital and -5.61 eV for the beta spin orbital.

In Table 3.3, we show the values of $t_{\nu\nu'}$ (off-diagonal terms) and $\varepsilon_{d\nu}$ (diagonal terms) in eV for alpha spin orbital. We obtain this table thanks to Fock matrix in the orthogonal atomic orbitals (FNAO).

In Table 3.4, we show the values of $t_{\nu\nu'}$ (off-diagonal terms) and $\varepsilon_{d\nu}$ (diagonal

Table 3.3. The values of $t_{\nu\nu'}$ (off-diagonal terms) and $\varepsilon_{d\nu}$ (diagonal terms) of $3d$ orbitals in terms of eV for the alpha spin orbital.

Alpha S.O.	$3z^2$-r^2	xy	yz	x^2-y^2	xz
$3z^2$-r^2	-6.32665	0.01361	-0.00816	0.00544	-0.00816
xy	0.01361	-6.32937	-0.00816	0.02449	0.00544
yz	-0.00816	-0.00816	-6.29672	-0.00544	0.00272
x^2-y^2	0.00544	0.02449	-0.00544	-6.32937	-0.02449
xz	-0.00816	0.00544	0.00272	0.02449	-6.34570

terms) in eV for beta spin orbital. We obtain this table thanks to Fock matrix in the orthogonal atomic orbitals (FNAO).

Table 3.4. The values of $t_{\nu\nu'}$ (off-diagonal terms) and $\varepsilon_{d\nu}$ (diagonal terms) of $3d$ orbitals in terms of eV for the beta spin orbital.

Beta S.O.	$3z^2$-r^2	xy	yz	x^2-y^2	xz
$3z^2$-r^2	-6.24502	-0.00816	-0.00544	0.00544	0. 00544
xy	-0.00816	-6.22597	0.01088	0.02449	0.00816
yz	-0.00544	0.01088	-6.22869	0.00816	0.01361
x^2-y^2	0.02449	0.02449	0.00816	-6.25590	-0.01361
xz	0.00544	0.00816	0.01361	-0.01361	-6.28583

In Table 3.5, we show the values of occupancies and eigenvalues of the $3d$ orbitals for the alpha spin orbital. We obtain these values from the natural population analysis.

In Table 3.6, we show the values of occupancies and eigenvalues of the $3d$ orbitals for the beta spin orbital. We obtain these values from the natural population analysis.

In table 3.7, we show the values of magnetization which is the difference between the occupancies of alpha spin and beta spin.

Table 3.5. The values of occupancies and eigenvalues of the $3d$ orbitals for the alpha spin orbital.

Alpha Spin Orbitals		
3d orbitals	**ε_d (eV)**	**$\langle n_{v\uparrow} \rangle$**
$3z^2$-r^2	-6.32665	0.88493
xy	-6.32937	0.84360
yz	-6.29672	0.74559
x^2-y^2	-6.32937	0.70275
xz	-6.34570	0.55391

Table 3.6. The values of occupancies and eigenvalues of the $3d$ orbitals for the beta spin orbital.

Beta Spin Orbitals		
3d orbitals	**ε_d (eV)**	**$\langle n_{v\downarrow} \rangle$**
$3z^2$-r^2	-6.24502	0.86403
xy	-6.22597	0.80766
yz	-6.22869	0.73676
x^2-y^2	-6.25590	0.69030
xz	-6.28583	0.55162

Table 3.7. The values of magnetization is the difference between the occupancies of $3d$ orbitals for alpha spin and beta spin.

3d orbitals	**Alpha Spin Occupancy $\langle n_{v\uparrow} \rangle$**	**Beta Spin Occupancy $\langle n_{v\downarrow} \rangle$**	**Magnetization $\langle M_v^z \rangle = \langle n_{v\uparrow} \rangle - \langle n_{v\downarrow} \rangle$**
$3z^2$-r^2	0.88493	0.86403	0.02090
xy	0.84360	0.80766	0.03594
yz	0.74559	0.73676	0.00883
x^2-y^2	0.70275	0.69030	0.01245
xz	0.55391	0.55162	0.00229

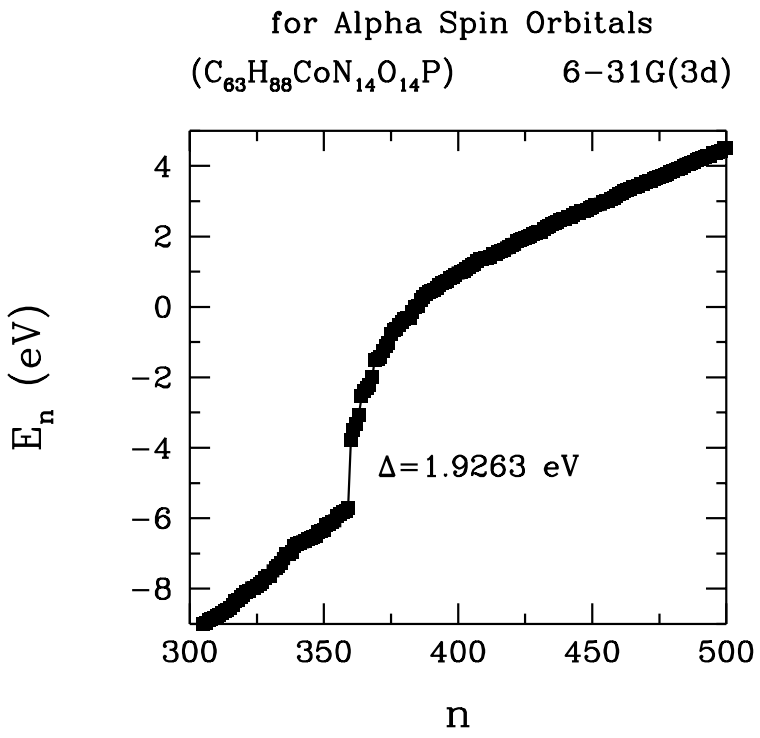

Figure 3.20. Energy eigenvalues E_n versus n for vitamin B_{12}. The forbidden energy gap (Δ) is approximately 1.93 eV between the HOMO and LUMO bands for alpha spin orbital. Here, n is the number of basis functions; $n = 1, 2, \cdots, N$.

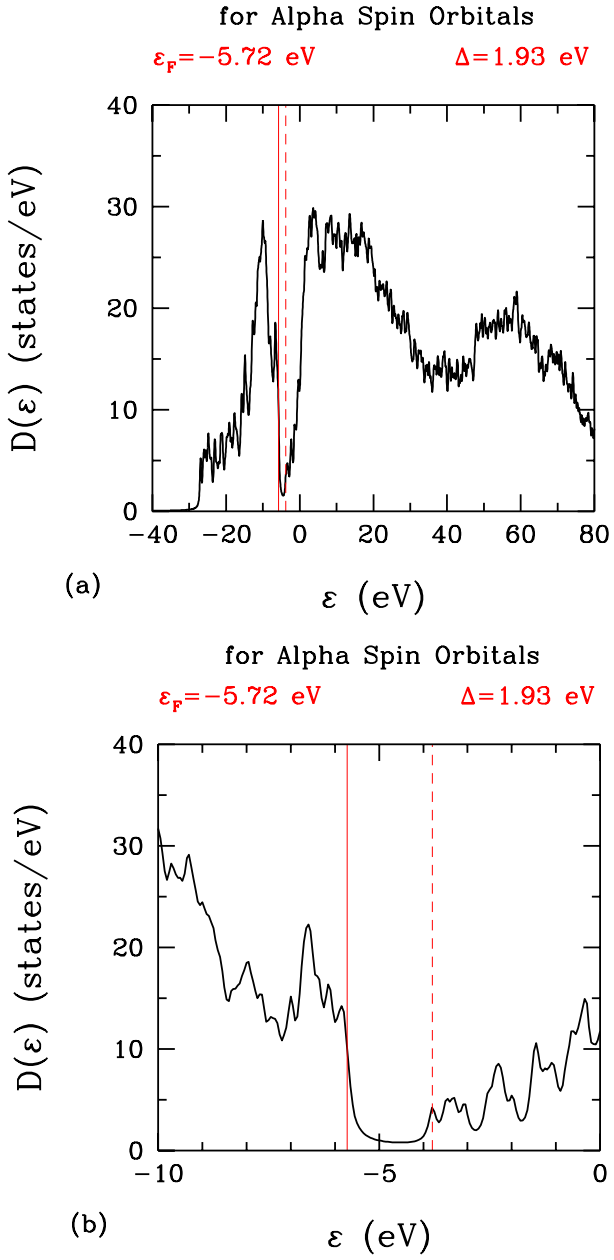

Figure 3.21. For all orbitals density of states $D(\varepsilon)$ versus ε are calculated by using Eq.(3.17) for alpha spin orbital. (a) The calculated density of state (DOS) of the vitamin B_{12} is plotted for $\gamma = 0.2$. (b) The x-axis is reduced in the range from -10 to 0 in order to demonstrate HOMO-LUMO region in much detail. This figure is broaden with ($\gamma = 0.1$). These plots are for 6-31G(3d) basis set. Here, the red solid line is the Fermi energy, at the same time, this line is the value of HOMO and also the red dashed line is the value of LUMO. In addition, these red lines are correspond to the values of HOMO and LUMO in the other figures.

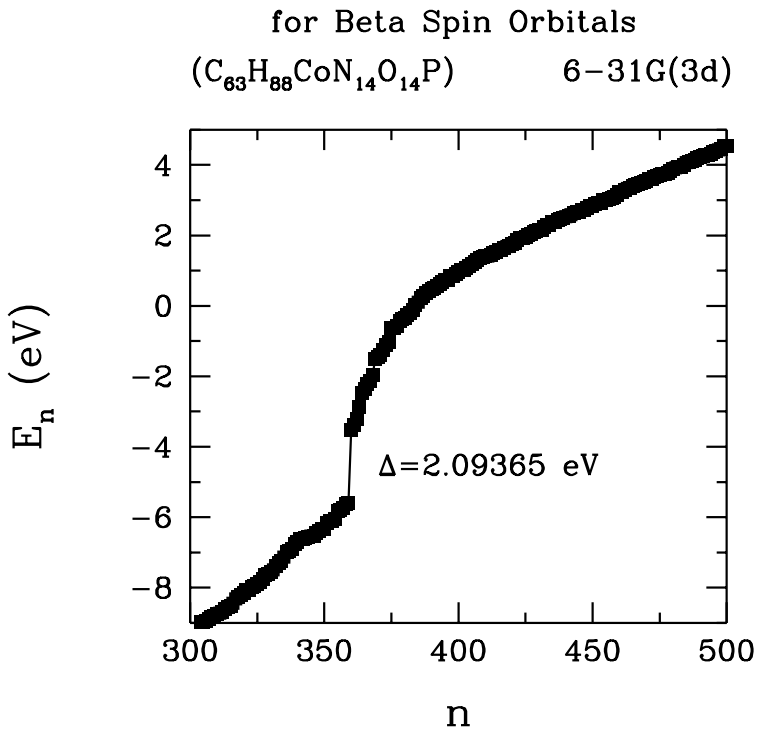

Figure 3.22. Energy eigenvalues E_n versus n for vitamin B_{12}. The forbidden energy gap (Δ) is approximately 2.09 eV between the HOMO and LUMO bands for beta spin orbital. Here, n is the number of basis functions; $n = 1, 2, \cdots, N$.

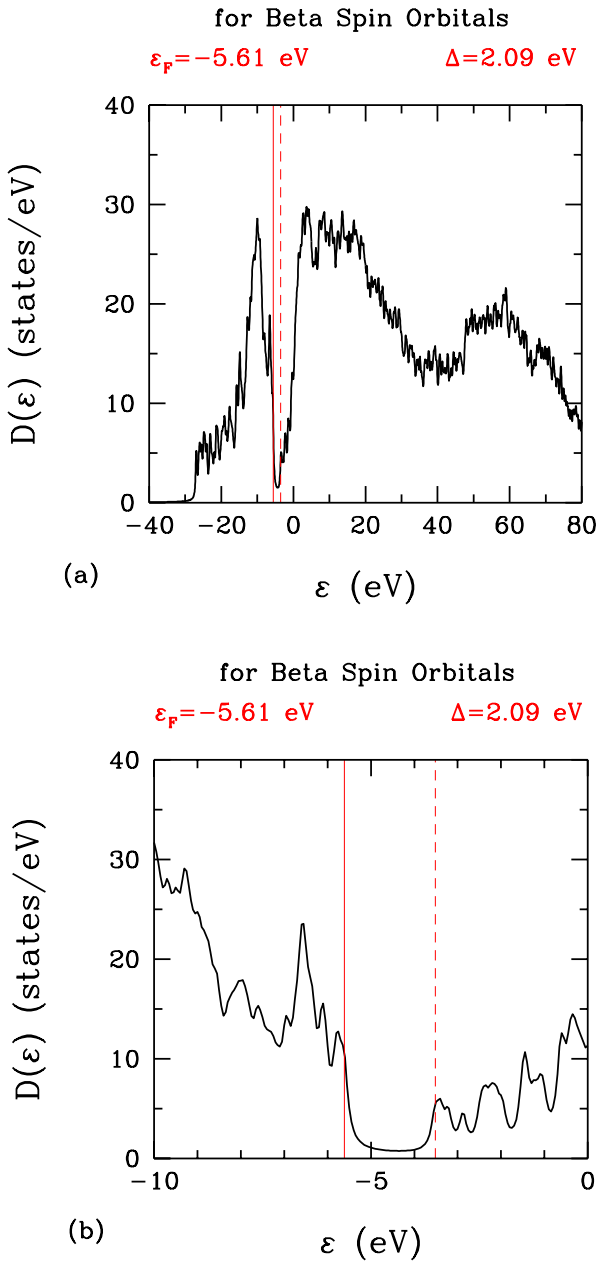

Figure 3.23. For all orbitals density of states $D(\varepsilon)$ versus ε are calculated by using Eq.(3.17) for beta spin orbital. (a) The calculated density of state (DOS) of the vitamin B_{12} is plotted for $\gamma = 0.2$. (b) The x-axis is reduced in the range from -10 to 0 in order to demonstrate HOMO-LUMO region in much detail. This figure is broaden with ($\gamma = 0.1$). These plots are for 6-31G(3d) basis set. Here, the red solid line is the Fermi energy, at the same time, this line is the value of HOMO and also the red dashed line is the value of LUMO. In addition, these red lines are correspond to the values of HOMO and LUMO in the other figures.

CHAPTER 4

CONCLUSIONS

In this thesis, we have obtained the electronic structure, molecular orbital wavefunction and energy eigenvalues of the vitamin B_{12} by using the density functional theory (DFT) via the Gaussian program. For vitamin B_{12}, some of the articles have done various calculations like optimization, energy and frequency by using various methods and basis sets [19, 30, 35] and we do optimization and energy calculation. The aim of my thesis is to constitute an effective Anderson model. Here, the $3d$ orbitals of cobalt atom corresponds to the magnetic impurity part in Anderson model, while the rest orbitals of the molecule can be considered as the host part of the Anderson model. To construct the multi-orbital Anderson model Hamiltonian, we have used the density functional theory and calculated the impurity ($\varepsilon_{d\nu}$) and the host energy (ε_m) levels as well as the hybridization matrix elements ($V_{\nu m}$) among these.

Firstly, in this study, the vitamin B_{12} has been optimized by using the DFT at the hybrid functional B3LYP level with LANL2DZ basis set for cobalt atom and 6-31G(3d) basis set for the rest orbitals of the atoms. After optimization, the Gaussian program gives us the correct electronic structure of vitamin B_{12}.

Output file which is obtained by the Gaussian program can be used as input file for new calculations in GaussView molecular visualization program. This is one of the most important properties of GaussView program. Thus, the output file which is obtained from the optimization is constituted our input file and this input file is opened by GaussView. Then, we make the energy calculation by adding FNAO and NAOMO keywords, basis sets, and DFT/B3LYP hybrid functional. Here, we use the natural atomic orbital (See Section 3.1) in order to dissociate the host part and the impurity part (only $3d$ orbitals) easily. The Gaussian program gives us molecular orbitals (in terms of atomic orbitals) and eigenvalues of any molecule without using any keywords.

We can obtain the Fock matrix, molecular orbital coefficients and bond analysis of any molecule thanks to NBO program which is attached to Gaussian program. Thus, we obtain the Fock matrix of vitamin B_{12} in terms of orthogonal atomic orbitals (FNAO). NAOMO and AOMO keywords give the molecular orbitals in the orthogonal atomic orbital and atomic orbital basis (See Section 3.1), respectively.

After we obtain the Fock matrix, we divide the Fock matrix into impurity part (on-

ly $3d$ orbitals of cobalt atom) and host part (the rest of orbitals) to find the hybridization terms of the $3d$ orbitals of cobalt atom. The impurity part directly gives us the diagonal term ($\varepsilon_{d\nu}$, the effective energies of $3d$ orbitals) and the off-diagonal term ($t_{\nu\nu'}$, the hopping energies between $3d$ orbitals). In addition, the values of occupancies and eigenvalues of $3d$ orbitals are shown by using the natural population analysis (See Table 3.2). Furthermore, in Section 3.2, we obtain that the energy gap is approximately 2.71 eV. Therefore, we find that the vitamin B_{12} exhibits semiconductor properties. We draw the density of states for all orbitals. After the host part is diagonalized, we obtain the energy eigenvalues of the host part ε_m and the eigenstates of the host part u_m without the $3d$ orbitals. Moreover, by using these values we draw the density of states without $3d$ orbitals, and we put the energy values of the $3d$ orbitals, the HOMO value and the LUMO value in figure. Thus, we see that the energy values of the $3d$ orbitals are below the Fermi level which is known as the HOMO value. As soon as we calculate the hybridization matrix elements between the host and the impurity part, we display separately the hybridization terms for each $3d$ orbitals in detail. Then, we construct the new Hamiltonian to check our calculations. After we diagonalize the new Hamiltonian, we obtain its new eigenvalues. We see that the new eigenvalues are equal to the eigenvalues which is obtained by Gaussian program.

We obtain the effective energies of $3d$ orbitals $\varepsilon_{d\nu}$, the Fermi levels μ, the energy eigenvalues of the host part ε_m and the impurity-host hybridization matrix elements $V_{\nu m}$ for the effective multi-orbital Anderson model.

We find out that the electron numbers of $3d$ orbitals are greater than or approximately equal to 1. The $3d$ orbitals of cobalt atom which is almost full occupation has not physical meaning to us. Therefore, we calculate the electron numbers of $3d$ orbitals by using LSDA method.

For LSDA spin polarized method, we achieve the density of state and energy. Here we calculate separately alpha spin and beta spin orbitals. We obtain that the energy gap is 1.93 eV for alpha spin orbital and 2.09 eV for beta spin orbitals. The energy gap of the cyanocobalamin is 1.96 eV as the computational value [17, 20, 38, 39]. We obtain the electron numbers and the magnetic moment of $3d$ orbitals. Here, we realize that the electron numbers of $3d$ orbitals are less than 1 for each spin orbitals and the total of the electron numbers of $3d$ orbitals is greater than or nearly equal to 1 for alpha plus beta spin orbitals.

Although the energy gap which has been obtained by LSDA is closed to the computational value, we achieve more correct results with B3LYP for the energy eigenvalues

of $3d$ orbitals, the density of states and the impurity-host hybridization matrix elements. The B3LYP has already been one of the most common used hybrid functional method in the literature due to the fact that it includes the contributions of different exchange and correlation energies. This information increases the accuracy of our results.

REFERENCES

[1] V. Rajapandian. *Computational Study on the Structure-Function Relationship in Copper Binding Proteins*. PhD thesis, University OF Madras, India, 2011.

[2] Yi Lu, Natasha Yeung, Nathan Sieracki, and Nicholas M Marshall. Design of functional metalloproteins. *Nature*, 460(7257):855–862, 2009.

[3] Felix Tuczek. Handbook of metalloproteins. vol. 3. edited by albrecht messerschmidt, wolfram bode and mirek cygler. *Angewandte Chemie International Edition*, 43(40):5290–5290, 2004.

[4] Ivano Bertini and Astrid Sigel. *Handbook on metalloproteins*. CRC Press, 2001.

[5] Kevin J Waldron, Julian C Rutherford, Dianne Ford, and Nigel J Robinson. Metalloproteins and metal sensing. *Nature*, 460(7257):823–830, 2009.

[6] Edit Y Tshuva, Stephen J Lippard, et al. Synthetic models for non-heme carboxylate-bridged diiron metalloproteins: strategies and tactics. *Chemical Reviews-Columbus*, 104(2):987–1012, 2004.

[7] Pawel M Kozlowski, Thomas G Spiro, and Marek Z Zgierski. Dft study of structure and vibrations in low-lying spin states of five-coordinated deoxyheme model. *The Journal of Physical Chemistry B*, 104(45):10659–10666, 2000.

[8] Meng-Sheng Liao, Ming-Ju Huang, and John D Watts. Iron porphyrins with different imidazole ligands. a theoretical comparative study. *The Journal of Physical Chemistry A*, 114(35):9554–9569, 2010.

[9] Mariusz Radon and Kristine Pierloot. Binding of co, no, and o2 to heme by density functional and multireference ab initio calculations. *The Journal of Physical Chemistry A*, 112(46):11824–11832, 2008.

[10] Damián A Scherlis, Matteo Cococcioni, Patrick Sit, and Nicola Marzari. Simulation of heme using dft+ u: a step toward accurate spin-state energetics. *The Journal of Physical Chemistry B*, 111(25):7384–7391, 2007.

[11] Damián A Scherlis and Darío A Estrin. Structure and spin-state energetics of an iron porphyrin model: An assessment of theoretical methods. *International journal of quantum chemistry*, 87(3):158–166, 2002.

[12] Yong Zhang, Hiroshi Fujisaki, and John E Straub. Direct evidence for mode-specific vibrational energy relaxation from quantum time-dependent perturbation theory. i. five-coordinate ferrous iron porphyrin model. *The Journal of chemical physics*,

130:025102, 2009.

[13] Md. Ehesan Ali, Biplab Sanyal, and Peter M. Oppeneer. Electronic structure, spin-states, and spin-crossover reaction of heme-related fe-porphyrins: A theoretical perspective. *The Journal of Physical Chemistry B*, 116(20):5849–5859, 2012.

[14] Hisashi Shimakoshi and Yoshio Hisaeda. Environmental-friendly catalysts learned from vitamin b12-dependent enzymes. *TCIMAIL*, 138:2–11, 2009.

[15] Carme Rovira and Pawel M Kozlowski. First principles study of coenzyme b12. crystal packing forces effect on axial bond lengths. *The Journal of Physical Chemistry B*, 111(12):3251–3257, 2007.

[16] Harald Solheim, Karina Kornobis, Kenneth Ruud, and Pawel M Kozlowski. Electronically excited states of vitamin b12 and methylcobalamin: Theoretical analysis of absorption, cd, and mcd data. *The Journal of Physical Chemistry B*, 115(4):737–748, 2010.

[17] EZ Kurmaev, A Moewes, L Ouyang, L Randaccio, P Rulis, WY Ching, M Bach, and M Neumann. The electronic structure and chemical bonding of vitamin b12. *EPL (Europhysics Letters)*, 62(4):582, 2003.

[18] Martin Stillman. Lecture note: The role of cobalt in vitamin b12, August 2010.

[19] Tommy Liljefors Kasper P. Jensen, Stephan P. A. Sauer and Per-Ola Norrby. Theoretical investigation of steric and electronic effects in coenzyme b12 models. *Organometallics*, 20:550–556, 2001.

[20] Lizhi Ouyang, L Randaccio, P Rulis, EZ Kurmaev, A Moewes, and WY Ching. Electronic structure and bonding in vitamin b_{12}, cyanocobalamin. *Journal of Molecular Structure: THEOCHEM*, 622(3):221–227, 2003.

[21] F.D.M. Haldane and P.W. Anderson. Simple model of multiple charge states of transition-metal impurities in semiconductors. *Physical Review B*, 13:2553–2559, 1976.

[22] M. J. Frisch, G. W. Trucks, H. B. Schlegel, G. E. Scuseria, M. A. Robb, J. R. Cheeseman, G. Scalmani, V. Barone, B. Mennucci, G. A. Petersson, H. Nakatsuji, M. Caricato, X. Li, H. P. Hratchian, A. F. Izmaylov, J. Bloino, G. Zheng, J. L. Sonnenberg, M. Hada, M. Ehara, K. Toyota, R. Fukuda, J. Hasegawa, M. Ishida, T. Nakajima, Y. Honda, O. Kitao, H. Nakai, T. Vreven, J. A. Montgomery, Jr., J. E. Peralta, F. Ogliaro, M. Bearpark, J. J. Heyd, E. Brothers, K. N. Kudin, V. N. Staroverov, R. Kobayashi, J. Normand, K. Raghavachari, A. Rendell, J. C. Burant, S. S. Iyengar, J. Tomasi, M. Cossi, N. Rega, J. M. Millam, M. Klene, J. E. Knox, J. B. Cross, V. Bakken, C. Adamo, J. Jaramillo, R. Gomperts, R. E. Stratmann, O. Yazyev, A. J. Austin, R. Cammi, C. Pomelli, J. W. Ochterski, R. L. Martin, K. Morokuma, V. G.

Zakrzewski, G. A. Voth, P. Salvador, J. J. Dannenberg, S. Dapprich, A. D. Daniels, Ö. Farkas, J. B. Foresman, J. V. Ortiz, J. Cioslowski, and D. J. Fox. Gaussian 09 Revision A.1. Gaussian Inc. Wallingford CT 2009.

[23] J. E. Carpenter E. D. Glendening, A. E. Reed and F. Weinhold. Nbo version 3.1.

[24] Alan E. Reed, Larry A. Curtiss, and Frank Weinhold. Intermolecular interactions from a natural bond orbital, donor-acceptor viewpoint. *Chemical Reviews*, 88(6):899–926, 1988.

[25] Roy Dennington, Todd Keith, and John Millam. Gaussview Version 5, 2009. Semichem Inc. Shawnee Mission KS.

[26] P Jeffrey Hay and Willard R Wadt. Ab initio effective core potentials for molecular calculations. potentials for the transition metal atoms sc to hg. *The Journal of chemical physics*, 82:270, 1985.

[27] Peter M Oppeneer, Pooja M Panchmatia, Biplab Sanyal, O Eriksson, and Md E Ali. Nature of the magnetic interaction between fe-porphyrin molecules and ferromagnetic surfaces. *Progress in Surface Science*, 84(1):18–29, 2009.

[28] Ruma Banerjee and Stephen W Ragsdale. The many faces of vitamin b12: Catalysis by cobalamin-dependent enzymes 1. *Annual review of biochemistry*, 72(1):209–247, 2003.

[29] Christian Kandt, Zhitao Xu, and D Peter Tieleman. Opening and closing motions in the periplasmic vitamin b12 binding protein btuf. *Biochemistry*, 45(44):13284–13292, 2006.

[30] Karina Kornobis, Neeraj Kumar, Bryan M. Wong, Piotr Lodowski, Maria Jaworska, Tadeusz Andruniów, Kenneth Ruud, and Pawel M. Kozlowski. Electronically excited states of vitamin b12: Benchmark calculations including time-dependent density functional theory and correlated ab initio methods. *The Journal of Physical Chemistry A*, 115(7):1280–1292, 2011.

[31] Joseph J Shiang, Allwyn G Cole, Roseanne J Sension, Kun Hang, Yuxiang Weng, Jenna S Trommel, Luigi G Marzilli, and Tianquan Lian. Ultrafast excited-state dynamics in vitamin b12 and related cob (iii) alamins. *Journal of the American Chemical Society*, 128(3):801–808, 2006.

[32] Troy A Stich, Amanda J Brooks, Nicole R Buan, and Thomas C Brunold. Spectroscopic and computational studies of co3+-corrinoids: spectral and electronic properties of the b12 cofactors and biologically relevant precursors. *Journal of the American Chemical Society*, 125(19):5897–5914, 2003.

[33] Nicole Dölker, Feliu Maseras, and Agusti Lledos. Density functional study on the ef-

fect of the trans axial ligand of b12 cofactors on the heterolytic cleavage of the co-c bond. *The Journal of Physical Chemistry B*, 107(1):306–315, 2003.

[34] Karl Gruber, Riikka Reitzer, and Christoph Kratky. Radical shuttling in a protein: Ribose pseudorotation controls alkyl-radical transfer in the coenzyme b12 dependent enzyme glutamate mutase. *Angewandte Chemie International Edition*, 40(18):3377–3380, 2001.

[35] Piotr Lodowski, Maria Jaworska, Karina Kornobis, Tadeusz Andruniów, and Pawel M. Kozlowski. Electronic and structural properties of low-lying excited states of vitamin b12. *The Journal of Physical Chemistry B*, 115(45):13304–13319, 2011.

[36] S Muthu and E Isac Paulraj. Journal of chemical and pharmaceutical research. *J. Chem*, 3(5):323–339, 2011.

[37] Prof. Ephraim Eliav. Introduction to quantum chemistry - appendix - 2. The School of Chemistry, Faculty of Exact Sciences, Tel Aviv University, Israel.

[38] Lizhi Ouyang, Paul Rulis, WY Ching, Giorgio Nardin, and Lucio Randaccio. Accurate redetermination of the x-ray structure and electronic bonding in adenosylcobalamin. *Inorganic chemistry*, 43(4):1235–1241, 2004.

[39] Kenneth L Brown et al. Chemistry and enzymology of vitamin b12. *Chemical Reviews-Columbus*, 105(6):2075–2150, 2005.

[40] Rickard Armiento. Density functional theory for systems with electronic edges. Master's thesis, Royal Institute of Technology, Stockholm, Sweden, 2000.

[41] Klaus Capelle. A bird's-eye view of density-functional theory. *Brazilian Journal of Physics*, 36:1318 – 1343, 12 2006.

[42] Michael P Marder. *Condensed matter physics*. Wiley, 2010.

[43] Ozan ARI. Electronic, spintronic and transport properties of carbon based nanowires. Master's thesis, İzmir Institute of Technology, 2011.

[44] Richard M Martin. *Electronic structure: basic theory and practical methods*. Cambridge university press, 2004.

[45] Frank Jensen. *Introduction to computational chemistry*. Wiley, 2007.

[46] Navid Abedi Khaledi. Linear response functions of solids within time-dependent density functional theory (tddft). Master's thesis, University of the Basque Country, 2011.

[47] M. Born and R. Oppenheimer. Zur quantentheorie der molekeln. *Annalen der Physik*,

389(20):457–484, 1927.

[48] JC Slater. Magnetic effects and the hartree-fock equation. *Physical Review*, 82(4):538, 1951.

[49] Llewellen H Thomas. The calculation of atomic fields. In *Mathematical Proceedings of the Cambridge Philosophical Society*, volume 23, pages 542–548. Cambridge Univ Press, 1927.

[50] Enrico Fermi. Eine statistische methode zur bestimmung einiger eigenschaften des atoms und ihre anwendung auf die theorie des periodischen systems der elemente. *Zeitschrift fü r Physik*, 48(1-2):73–79, 1928.

[51] P. Hohenberg and W. Kohn. Inhomogeneous electron gas. *Phys. Rev.*, 136:B864–B871, Nov 1964.

[52] W. Kohn and L. J. Sham. Self-consistent equations including exchange and correlation effects. *Phys. Rev.*, 140:A1133–A1138, Nov 1965.

[53] Paul Adrien Maurice Dirac. Quantum mechanics of many-electron systems. *Proceedings of the Royal Society of London. Series A, Containing Papers of a Mathematical and Physical Character*, 123(792):714–733, 1929.

[54] Prasanjit Samal. *Studies in Excited-State Density-Functional Theory*. PhD thesis, INDIAN INSTITUTE OF TECHNOLOGY, 2006.

[55] Robert O Jones and Olle Gunnarsson. The density functional formalism, its applications and prospects. *Reviews of Modern Physics*, 61(3):689, 1989.

[56] R.G. Parr and W. Yang. *Density Functional Theory of Atoms and Molecules*. Oxford University Press, New York, 1989.

[57] Hande Toffoli. Lecture iv : The hartree-fock method, March 2009.

[58] Hande Toffoli. Lecture vii : The hohenberg-kohn theorem and the kohn-sham equations, April 2009.

[59] Gustavo E Scuseria and Viktor N Staroverov. *Progress in the development of exchange-correlation functionals*. Elsevier, 2006.

[60] Gustavo E Scuseria and Viktor N Staroverov. Progress in the development of exchange-correlation functionals. *Theory and applications of computational chemistry: the first*, 40:669–724, 2005.

[61] NM Harrison. An introduction to density functional theory. *NATO SCIENCE SERIES SUB SERIES III COMPUTER AND SYSTEMS SCIENCES*, 187:45–70, 2003.

[62] Peter Haynes. *Linear-scaling methods in ab initio quantum-mechanical calculations "3.1 Density-functional theory"*. PhD thesis, University of Cambridge, 1998.

[63] WMC Sameera. *Electronic Structure of Transition Metal Ions and Clusters*. PhD thesis, University of Glasgow, 2008.

[64] Axel D Becke. A new mixing of hartree–fock and local density-functional theories. *The Journal of Chemical Physics*, 98:1372, 1993.

[65] Murray Gell-Mann and Keith A Brueckner. Correlation energy of an electron gas at high density. *Physical Review*, 106(2):364, 1957.

[66] WJ Carr Jr and AA Maradudin. Ground-state energy of a high-density electron gas. *Physical Review*, 133(2A):A371, 1964.

[67] P Nozieres and D Pines. Electron interaction in solids. characteristic energy loss spectrum. *Physical Review*, 113(5):1254, 1959.

[68] WJ Carr Jr. Energy, specific heat, and magnetic properties of the low-density electron gas. *Physical Review*, 122(5):1437, 1961.

[69] David M Ceperley and BJ Alder. Ground state of the electron gas by a stochastic method. *Physical Review Letters*, 45(7):566–569, 1980.

[70] S. H. Vosko, L. Wilk, and M. Nusair. Accurate spin-dependent electron liquid correlation energies for local spin density calculations: a critical analysis. *Canadian Journal of Physics*, 58(8):1200–1211, 1980.

[71] John P Perdew, Kieron Burke, and Matthias Ernzerhof. Generalized gradient approximation made simple. *Physical review letters*, 77(18):3865–3868, 1996.

[72] Seymur Changirov. Size and composition modulated superlattices of silicon base nanowires. Master's thesis, Bilkent University, 2008.

[73] A. D. Becke. Density-functional exchange-energy approximation with correct asymptotic behavior. *Phys. Rev. A*, 38:3098–3100, Sep 1988.

[74] Chengteh Lee, Weitao Yang, and Robert G. Parr. Development of the colle-salvetti correlation-energy formula into a functional of the electron density. *Phys. Rev. B*, 37:785–789, Jan 1988.

APPENDIX A

CALCULATION METHODS AND APPROXIMATIONS

A.1. Many-Body Problem

Our starting point is the time independent non-relativistic Schrödinger equation that defines a system of matter. In many-body systems one can solve an eigenvalue problem for the energy E in the form [40, 41]

$$H\Psi = E\Psi \ . \tag{A.1}$$

The Hamiltonian of a typical many-body system can be written as [42–45]

$$H = T_e + T_i + V_{ee} + V_{ii} + V_{ei} \ . \tag{A.2}$$

In Eq.(A.2), these terms separately define

$$T_e = -\frac{1}{2}\sum_{i=1}^{N} \nabla_{\mathbf{i}}^{\mathbf{2}} \tag{A.3}$$

where T_e is the electron kinetic energy;

$$T_i = -\frac{1}{2}\sum_{I=1}^{ions} \nabla_{\mathbf{I}}^{\mathbf{2}} \tag{A.4}$$

where T_i is the ion kinetic energy;

$$V_{ee} = \frac{1}{2}\sum_{i\neq j}^{N}\frac{1}{|\boldsymbol{r_i}-\boldsymbol{r_j}|} \tag{A.5}$$

where V_{ee} is the electron-electron repulsion term;

$$V_{ii} = \frac{1}{2}\sum_{I\neq J}^{ions}\frac{Z_I Z_J}{|\boldsymbol{R_I}-\boldsymbol{R_J}|} \tag{A.6}$$

where V_{ii} is the ion-ion repulsion term;

$$V_{ei} = -\sum_{i=1}^{N}\sum_{I=1}^{ions}\frac{Z_I}{|\boldsymbol{r_i}-\boldsymbol{R_I}|} \implies V_{ei} = \sum_{i=1}^{N} V_{ext}(\boldsymbol{r_i}) \tag{A.7}$$

where V_{ei} is the attractive interaction between the electrons and ions described as an external potential for the electrons.

In general, m_e and r_i are the electron mass and positions, respectively. M_I is the mass of the ion, R_I is the corresponding positions, and Z_I is the ion charge. The Hamiltonian form contains [42, 46]

$$\begin{aligned} H = &-\frac{1}{2}\sum_{i=1}^{N}\nabla_{\mathbf{i}}^{\mathbf{2}} - \frac{1}{2}\sum_{I=1}^{ions}\nabla_{\mathbf{I}}^{\mathbf{2}} + \frac{1}{2}\sum_{i\neq j}^{N}\frac{1}{|\boldsymbol{r_i}-\boldsymbol{r_j}|} \\ &+\frac{1}{2}\sum_{I\neq J}^{ions}\frac{Z_I Z_J}{|\boldsymbol{R_I}-\boldsymbol{R_J}|} + \sum_{i=1}^{N} V_{ext}(\boldsymbol{r_i})\ . \end{aligned} \tag{A.8}$$

Born-Oppenheimer or adiabatic approximation (1927) [47] is setting the mass of ion to infinity, then the kinetic energy of the ion and the ion-ion repulsion term can be neglected. Due to their masses the ions move much slower than the electrons so we can consider the electrons as moving in the field of fixed ions, therefore the nuclear kinetic energy is zero and their potential energy is merely a constant. As a result, the electronic Hamiltonian H reduces a sum of three contributions: the kinetic energy of the electrons

T_e, the external potential energy (the attraction between the electrons and ions) V_{ext}, and the internal potential energy (the repulsion between individual electrons) V_{ee}.

$$H = T_e + V_{ext} + V_{ee} \tag{A.9}$$

where H is the quantum mechanical Hamiltonian of the form:

$$H = -\frac{1}{2}\sum_{i=1}^{N}\nabla_i^2 + \sum_{i=1}^{N}V_{ext}(\boldsymbol{r_i}) + \frac{1}{2}\sum_{i\neq j}^{N}\frac{1}{|\boldsymbol{r_i}-\boldsymbol{r_j}|}\,, \tag{A.10}$$

$$H\Psi_n = \sum_{i=1}^{N}\left(-\frac{1}{2}\nabla_i^2 + V_{ext}(\boldsymbol{r_i})\right)\Psi_n + \frac{1}{2}\sum_{i\neq j}^{N}\frac{1}{|\boldsymbol{r_i}-\boldsymbol{r_j}|}\Psi_n \tag{A.11}$$

where Ψ_n is the many-body wavefunction, replaced by a set of N one-electron equations of the form. We express the wavefunction Ψ_n as a Slater determinant [48] of orbital wavefunctions $\{\psi_i(\boldsymbol{r}),\ i = 1, 2\ldots, N\}$ where N is the number of electrons, the energy functional is given by

$$\begin{aligned}
E &= \langle\Psi_n|H|\Psi_n\rangle \\
&= \sum_{i}^{N}\int d\boldsymbol{r}\psi_i^*(\boldsymbol{r})\left(-\frac{1}{2}\nabla_i^2 + V_{ext}(\boldsymbol{r_i})\right)\psi_i(\boldsymbol{r}) \\
&+ \frac{1}{2}\sum_{i\neq j}\int d\boldsymbol{r}d\boldsymbol{r'}\psi_i^*(\boldsymbol{r})\psi_i(\boldsymbol{r})\frac{1}{|\boldsymbol{r}-\boldsymbol{r'}|}\psi_j^*(\boldsymbol{r'})\psi_j(\boldsymbol{r'}) \\
&- \frac{1}{2}\sum_{i\neq j}\int d\boldsymbol{r}d\boldsymbol{r'}\psi_i^*(\boldsymbol{r})\psi_j^*(\boldsymbol{r'})\frac{1}{|\boldsymbol{r}-\boldsymbol{r'}|}\psi_i(\boldsymbol{r'})\psi_j(\boldsymbol{r})\,.
\end{aligned} \tag{A.12}$$

A.2. Density Functional Theory

The basis of density functional theory (DFT), in 1927, it proposed the first time by Thomas [49] and Fermi [50] , then Hohenberg and Kohn [51] based on their works and finally Kohn and Sham [52] improved and concluded their the whole works. The DFT, which is quite common, current and compatible with the experimental results is a method.

It is commonly a successful approach in order to determine the ground state properties of metals, semiconductors and insulators. Nowadays, it is known that the DFT has been used to calculate the binding energy of molecules and the band structure of solids in physics and chemistry. The aim of density functional theory, it represents the characteristics of the many-body system by using the ground state electron density without the wave functions.

A.2.1. Thomas-Fermi-Dirac Approximations

The original of DFT is proposed the first time in 1927 by Thomas [49] and Fermi [50]. They expressed the kinetic energy with respect to the electron density. Both Thomas and Fermi neglected exchange and correlation among the electrons. This was extended by Dirac [53] in 1930, who formulated the local approximation for exchange. This formulation for exchange is still in use today. In Thomas-Fermi-Dirac approximation, the energy functional is denoted as [41, 54–56]

$$E_{TFD}[\rho] = \frac{3}{10}(3\pi^2)^{2/3}\int d^3r\rho(\boldsymbol{r})^{5/3} + \int d^3rV_{ext}(\boldsymbol{r})\rho(\boldsymbol{r}) - \frac{3}{4}\left(\frac{3}{\pi}\right)^{1/3}\int d^3r\rho(\boldsymbol{r})^{4/3} + \frac{1}{2}\int d^3rd^3r'\frac{\rho(\boldsymbol{r})\rho(\boldsymbol{r'})}{|\boldsymbol{r}-\boldsymbol{r'}|} \quad . \tag{A.13}$$

In Eq.(A.13), the first term is the kinetic energy of a non-interacting homogeneous electron gas with the density ρ, the second term is the external potential, the third term is the local approximation of exchange energy, and the last term is the classical electrostatic Hartree energy (electron-electron Coulomb repulsion). However, the Thomas-Fermi-Dirac approach starts with approximations that are too crude, missing the essential physics. Therefore, it falls short of the goal of a useful description of electrons in matter.

A.2.2. Hohenberg-Kohn Theorems

The DFT is based on the existence of two remarkable theorems proven by Hohenberg and Kohn in 1964 [51]. Stated simply they are follows [56]:
Theorem I: For any system of N-interacting electrons in the external potential $V_{ext}(\boldsymbol{r})$ is determined by a unique functional of the ground state electron density $\rho(\boldsymbol{r})$ [43, 44, 57,

58].

$$V_{ext}(\boldsymbol{r}) \longleftrightarrow \rho(\boldsymbol{r}) \tag{A.14}$$

Theorem II: The global minimum value of energy functional is the ground state energy for any system and the electron density $\rho(\boldsymbol{r})$ that minimizes the functional energy is the ground state energy. The ground state energy can be obtained variationally [43, 44, 57, 58].

The electronic Hamiltonian of many-body system consists of a sum of three terms [43, 44, 55, 57, 58],

$$H = T_e + V_{ee} + V_{ext} \tag{A.15}$$

the electron kinetic energy, the electron-electron interaction and the interaction with the external potential (using Hartree atomic units $\hbar = m_e = e = 1/(4\pi\varepsilon_0) = 1$)

$$H = -\frac{1}{2}\sum_{i=1}^{N}\nabla_i^2 + \sum_{i=1}^{N}\sum_{i<j}^{N}\frac{1}{|\boldsymbol{r_i} - \boldsymbol{r_j}|} + \sum_{i=1}^{N}V_{ext}(\boldsymbol{r_i})\ . \tag{A.16}$$

Since $\rho(\boldsymbol{r})$ determines V_{ext}, it should also determine all properties of the ground state, including the kinetic energy of electrons and the energy of interaction among electrons, that is, the total ground state energy is a functional of density with the following:

$$E[\rho(\boldsymbol{r})] = T[\rho(\boldsymbol{r})] + V_{ee}[\rho(\boldsymbol{r})] + V_{ext}[\rho(\boldsymbol{r})]\ . \tag{A.17}$$

The energy functional $E[\rho(\boldsymbol{r})]$ referred to in the first Hohenberg-Kohn theorem [51] can be written with regard to the external potential $V_{ext}(\boldsymbol{r})$ in the following way,

$$E[\rho(\boldsymbol{r})] = F[\rho(\boldsymbol{r})] + \int \rho(\boldsymbol{r})V_{ext}(\boldsymbol{r})d^3r \tag{A.18}$$

where the external potential

$$V_{ext}(\boldsymbol{r}) = -\sum_{I}\frac{Z_I}{|\boldsymbol{r} - \boldsymbol{R_I}|} \tag{A.19}$$

is generated by the ions and $F[\rho(\boldsymbol{r})]$ is the unique functional of kinetic energy plus Coulomb interaction energy between electrons. Combining the external potential $V_{ext}(\boldsymbol{r})$, the corresponding ground state density $\rho(\boldsymbol{r})$ minimizes the functional under the constraint that the total number of electrons is kept fixed. Thus, the second Hohenberg-Kohn theorem provides a recipe for the calculation of the ground state density. It is suitable to separate out the classical Coulomb energy from $F[\rho(\boldsymbol{r})]$ and to write

$$F[\rho(\boldsymbol{r})] = T[\rho(\boldsymbol{r})] + \frac{1}{2}\int\int \frac{\rho(\boldsymbol{r})\rho(\boldsymbol{r'})}{|\boldsymbol{r}-\boldsymbol{r'}|} d^3r d^3r' \ . \tag{A.20}$$

Then, the expression for the energy functional Eq.(A.18) becomes

$$E[\rho(\boldsymbol{r})] = T[\rho(\boldsymbol{r})] + \int \rho(\boldsymbol{r}) V_{ext}(\boldsymbol{r}) d^3r + \frac{1}{2}\int\int \frac{\rho(\boldsymbol{r})\rho(\boldsymbol{r'})}{|\boldsymbol{r}-\boldsymbol{r'}|} d^3r d^3r' \ . \tag{A.21}$$

A.2.3. The Kohn-Sham Equations

In the previous section, provide a method of minimizing energy by changing corresponding density. In order to construct such an approximation, it has been proposed by Kohn and Sham (1965) [52] to introduce a reference system of N non-interacting electrons moving in an effective potential V_{eff}, where the electron density $\rho(\boldsymbol{r})$ agrees with the one of the interacting system. The ground state wavefunction of this reference system is simply given by the Slater [48] determinant of a set of N single-particle wavefunctions

$$\Psi_s = \frac{1}{\sqrt{N!}} det[\psi_1 \psi_2 \cdots \psi_N] \tag{A.22}$$

which satisfy the set of single-particle Schrödinger equations.

$$\left(-\frac{1}{2}\nabla^2 + V_{eff}(\boldsymbol{r})\right)\psi_i(\boldsymbol{r}) = \varepsilon_i \psi_i(\boldsymbol{r}) \tag{A.23}$$

which are called Kohn-Sham equation. The wavefunctions ψ_i are called Kohn-Sham wavefunctions. According to Pauli exclusion principle $(0 \leq n_i \leq 1)$, the ground state

density of this system is calculated in the following way:

$$\rho(\boldsymbol{r}) = \sum_{i}^{N} |\psi_i(\boldsymbol{r})|^2 \tag{A.24}$$

The expression for the energy functional of the non-interacting reference system is [59, 60]

$$E[\rho(\boldsymbol{r})] = T_s[\rho(\boldsymbol{r})] + \int V_{eff}\rho(\boldsymbol{r})d^3\boldsymbol{r} \tag{A.25}$$

where the subscript "s" stands for "single-particle". According to the second Hohenberg-Kohn theorem [51], the ground state of the reference system minimizes the energy functional $E[\rho(\boldsymbol{r})]$ under the constraint of fixed electron number. Using Lagrange multipliers ε_i to take these constraints into account the minimization of the energy functional $E[\rho(\boldsymbol{r})]$ reproduces the set of differential equations. They represented the total energy functional into the following that [56, 61],

$$E[\rho(\boldsymbol{r})] = T_s[\rho(\boldsymbol{r})] + V_{ext}[\rho(\boldsymbol{r})] + V_{ee}[\rho(\boldsymbol{r})] + E_{xc}[\rho(\boldsymbol{r})]\ . \tag{A.26}$$

For the energy functional of the interacting system we may write

$$E[\rho(\boldsymbol{r})] = T_s[\rho(\boldsymbol{r})] + \int \rho(\boldsymbol{r})V_{ext}d^3r + \frac{1}{2}\int\int \frac{\rho(\boldsymbol{r})\rho(\boldsymbol{r'})}{|\boldsymbol{r}-\boldsymbol{r'}|}d^3rd^3r' + E_{xc}[\rho(\boldsymbol{r})] \tag{A.27}$$

where $T_s[\rho(\boldsymbol{r})]$ is the kinetic energy of electrons which has the same density ρ in a system. This is considered as a system with non-interacting electrons. V_{ext} is the external potential and V_{ee} is the Coulomb interaction between electrons. The last functional, $E_{xc}[\rho(\boldsymbol{r})]$ is called the exchange-correlation energy.

A.2.4. The Roothaan-Hartree-Fock (RHF) Equations

According to variational principle [56, 61]

$$\delta\left(E[\rho] - \mu\int \rho(\boldsymbol{r})dr\right) = 0 \tag{A.28}$$

where μ is the Lagrange multiplier. In terms of variational derivatives

$$\frac{\delta E[\rho]}{\delta \rho(\boldsymbol{r})} = \mu \, . \tag{A.29}$$

Minimization of the energy functional Eq.(A.27) under the constraint of fixed number yields a second set of Schrödinger equation by using the variational principle [56, 61]

$$\mu = \frac{\delta E[\rho(\boldsymbol{r})]}{\delta \rho(\boldsymbol{r})} = \frac{\delta T_s[\rho(\boldsymbol{r})]}{\delta \rho(\boldsymbol{r})} + V_{ext}(\boldsymbol{r}) + \int \frac{\rho(\boldsymbol{r'})}{|\boldsymbol{r} - \boldsymbol{r'}|} d^3 r' + \frac{\delta E_{xc}[\rho(\boldsymbol{r})]}{\delta \rho(\boldsymbol{r})} \, . \tag{A.30}$$

Here we combined together all terms, excepting noninteracting electron kinetic energy into an effective potential $V_{eff}(\boldsymbol{r})$ depending on r

$$V_{eff}(\boldsymbol{r}) = V_{ext}(\boldsymbol{r}) + \int \frac{\rho(\boldsymbol{r'})}{|\boldsymbol{r} - \boldsymbol{r'}|} d^3 r' + V_{xc}(\boldsymbol{r}) \tag{A.31}$$

where the exchange correlation potential is defined as a functional derivative of the exchange correlation energy [62]

$$V_{xc}(\boldsymbol{r}) = \frac{\delta E_{xc}[\rho(\boldsymbol{r})]}{\delta \rho(\boldsymbol{r})} \, . \tag{A.32}$$

The DFT energy functional is minimized yielding the Kohn-Sham equations

$$\left[-\frac{1}{2} \nabla_i^2 + V_{ext}(\boldsymbol{r}) + \int d\boldsymbol{r'} \frac{\rho(\boldsymbol{r})}{|\boldsymbol{r} - \boldsymbol{r'}|} + V_{xc}(\boldsymbol{r}) \right] \psi_i(\boldsymbol{r}) = \varepsilon_i \psi_i(\boldsymbol{r}) \, . \tag{A.33}$$

The Fock operator for each electron can be defined as [45, 63]

$$F = -\frac{1}{2} \nabla_i^2 + V_{ext}(\boldsymbol{r}) + \int d\boldsymbol{r'} \frac{\rho(\boldsymbol{r})}{|\boldsymbol{r} - \boldsymbol{r'}|} + V_{xc}(\boldsymbol{r}) \tag{A.34}$$

and

$$F \psi_i(\boldsymbol{r}) = \varepsilon_i \psi_i(\boldsymbol{r}) \tag{A.35}$$

where $\psi_i(\boldsymbol{r})$ is an eigenfunction of the single-particle Hamiltonian F, the Fock operator and corresponding energy is ε_i . The local exchange potential is given as [56, 61]

$$V_{xc}(\boldsymbol{r}) = \frac{\delta E_{xc}^{LDA}}{\delta \rho(\boldsymbol{r})} = \epsilon_{xc}(\rho) + \rho(\boldsymbol{r}) \frac{\delta \epsilon_{xc}}{\delta \rho(\boldsymbol{r})} \ . \tag{A.36}$$

In order to solve the Kohn-Sham equations the molecular orbitals $\psi_i(\boldsymbol{r})$ are expanded in terms of atomic orbitals $\phi_\xi(\boldsymbol{r})$,

$$\psi_i(\boldsymbol{r}) = \sum_{\xi=1}^{N} \beta_{i\xi} \ \phi_\xi(\boldsymbol{r}) \tag{A.37}$$

and we substitute this expansion into Eq.(A.33) and take the inner product with ϕ_ξ [45, 63]

$$\sum_{\xi',\xi=1}^{N} \beta_{i\xi} \langle \phi_\xi | F | \phi_{\xi'} \rangle = \varepsilon_i \sum_{\xi',\xi=1}^{N} \beta_{i\xi} S_{\xi,\xi'} \tag{A.38}$$

where the overlap matrix is

$$S_{\xi,\xi'} = \langle \phi_\xi | \phi_{\xi'} \rangle, \quad \text{for } \ i = 1, 2, \ldots, N; \ \xi, \xi' = 1, 2, \ldots, N \ . \tag{A.39}$$

The electron density is calculated accordingly from [56, 61]

$$\rho(\boldsymbol{r}) = \sum_{i=1}^{n_{occ}} n_i |\psi_i(\boldsymbol{r})|^2 \ . \tag{A.40}$$

Here $n_i = 0, 1$ is the occupation number and $i = 1, 2, \ldots, n_{occ} < N$.

The Eq.(A.38) can also be obtained for the Hartree-Fock equations [64], and they are called the Roothaan-Hartree-Fock (RHF) equations. Furthermore, these N equations can be collectively represented by matrix equations [45],

$$\underset{\sim}{\boldsymbol{F}} \cdot \underset{\sim}{\boldsymbol{\beta}} \ = \ \underset{\sim}{\boldsymbol{\varepsilon}} \cdot \underset{\sim}{\boldsymbol{S}} \cdot \underset{\sim}{\boldsymbol{\beta}} \tag{A.41}$$

where $\underset{\sim}{\varepsilon}$ is a diagonal matrix of the orbital energies ε_i, and $\underset{\sim}{S}$ is the overlap matrix, $S_{\xi,\xi'} = \langle\phi_\xi|\phi_{\xi'}\rangle$. The $\underset{\sim}{F}$ matrix contains the Fock matrix elements, $F_{\xi,\xi'} = \langle\phi_\xi|F|\phi_{\xi'}\rangle$, and β is a $N \times N$ matrix of molecular orbital coefficients $\beta_{i\xi}$.

A.2.5. The Kohn-Sham Scheme

The idea of the Kohn-Sham method is best understood as follows [59, 60]. Consider a generalized Hamiltonian after the Born-Oppenheimer approximation

$$H = T + V_{ext} + V_{ee} \ , \tag{A.42}$$

$$H = \sum_i^N \left(-\frac{1}{2}\nabla_i^2 + V_{ext}(\boldsymbol{r}_i) \right) + \sum_{i<j}^N \frac{1}{|\boldsymbol{r_i} - \boldsymbol{r_j}|} \tag{A.43}$$

in which the term V_{ee} is scaled by an electron-electron coupling constant λ. We are interested in values of λ between 0 and 1.

In Levy's constraint search formulation of the Hohenberg-Kohn principle, this is stated as [59, 60]

$$F_\lambda[\rho] = \langle \Psi_\rho^{min,\lambda} | \left(T + \lambda V_{ee}\right) | \Psi_\rho^{min,\lambda} \rangle \tag{A.44}$$

where $\Psi_\rho^{min,\lambda}$ is the N-electron wave function.

For real system, $\lambda = 1$, so that $F_1[\rho] = F[\rho]$ is the universal function. This is the complicated problem to solve. The value $\lambda = 0$ corresponds to a system of noninteracting electrons moving in the external potential $V_{ext}(\boldsymbol{r})$. The noninteracting Schrödinger equation is solvable. The solution is $\psi_0 = \Psi_\rho^{min,0}$ a single Slater determinant of one-electron wave functions obtained from the single-particle equations [56, 61]

$$\left[-\frac{1}{2}\nabla_i^2 + V_{ext}(\boldsymbol{r}_i) \right] \psi_i(\boldsymbol{r}) = \varepsilon_i \psi_i(\boldsymbol{r}) \ . \tag{A.45}$$

The universal density functional for this noninteracting system is thus [59, 60]

$$F_0[\rho] = T_s[\rho] = -\frac{1}{2}\sum_i^N \langle \psi_i | \nabla^2 | \psi_i \rangle \tag{A.46}$$

where the density is given by

$$\rho(\boldsymbol{r}) = \sum_{i}^{N} |\psi_i(\boldsymbol{r})|^2 \ . \tag{A.47}$$

For a noninteracting system,

$$F_1[\rho] = F[\rho] = T_s[\rho] + J[\rho] + E_{xc}[\rho] \tag{A.48}$$

where $J[\rho]$ is the Coulomb repulsion energy

$$J[\rho] = \frac{1}{2} \int \frac{\rho(\boldsymbol{r}_i)\rho(\boldsymbol{r}_j)}{|\boldsymbol{r_i} - \boldsymbol{r_j}|} d\boldsymbol{r}_i d\boldsymbol{r}_j \ . \tag{A.49}$$

A.2.6. Exchange-Correlation Functionals

In practical Kohn-Sham DFT, the exchange-correlation functional E_{xc} is usually divided into two parts as exchange and correlation functionals [56, 61]

$$E_{xc}[\rho(\boldsymbol{r})] = E_x[\rho(\boldsymbol{r})] + E_c[\rho(\boldsymbol{r})] \ . \tag{A.50}$$

Using the Hellman-Feynman theorem as follows [59, 60]

$$\frac{\partial F_\lambda[\rho]}{\partial \lambda} = \langle \Psi_\rho^{min,\lambda} | V_{ee} | \Psi_\rho^{min,\lambda} \rangle \ \ , \tag{A.51}$$

$$\int_0^1 \frac{\partial F_\lambda[\rho]}{\partial \lambda} d\lambda = \int_0^1 \langle \Psi_\rho^{min,\lambda} | V_{ee} | \Psi_\rho^{min,\lambda} \rangle d\lambda \ \ , \tag{A.52}$$

$$F_1[\rho] - F_0[\rho] = T_s[\rho] + J[\rho] + E_{xc}[\rho] - T_s[\rho]$$
$$= E_{xc}[\rho] + J[\rho] \, . \tag{A.53}$$

Thus, we obtain the adiabatic connection formula

$$E_{xc}[\rho] = \int_0^1 \langle \Psi_\rho^{min,\lambda} | V_{ee} | \Psi_\rho^{min,\lambda} \rangle d\lambda - J[\rho] \, . \tag{A.54}$$

The exchange energy is defined by

$$E_x[\rho] = \langle \Phi_\rho^{min} | V_{ee} | \Phi_\rho^{min} \rangle - J[\rho] \tag{A.55}$$

where Φ_ρ^{min} is the Kohn-Sham determinant, while the correlation energy is taken formally as the difference [59, 60]

$$E_c[\rho] = E_{xc}[\rho] - E_x[\rho] = \langle \Psi_\rho^{min} | V_{ee} | \Psi_\rho^{min} \rangle - \langle \Phi_\rho^{min} | V_{ee} | \Phi_\rho^{min} \rangle \tag{A.56}$$

where Ψ_ρ^{min} is the exact interacting wave function.

A.2.6.1. Local Density Approximation (LDA)

The local density approximation consists in applying the exact results of the theory of a uniform electron gas to real nonuniform densities. Generally, the LDA is any approximation of the form

$$E_{xc}^{LDA}[\rho] = \int \rho(\boldsymbol{r}) \epsilon_{xc}(\rho) d\boldsymbol{r} \tag{A.57}$$

where $\epsilon_{xc}(\rho) = \epsilon_x(\rho) + \epsilon_c(\rho)$ is the exchange-correlation energy per particle of the electron gas, which is a function of the density only [46, 59, 60].

The LDA exchange energy is

$$E_x^{LDA} = -C_x \int \rho^{4/3}(\boldsymbol{r}) d\boldsymbol{r} \tag{A.58}$$

where $C_x = \frac{3}{4}\left(\frac{3}{\pi}\right)^{1/3}$. The LDA exchange energy per particle is

$$\begin{aligned} \epsilon_x^{LDA}(\rho) &= -C_x \rho^{1/3} \\ &= -\frac{3}{4}\left(\frac{3}{2\pi}\right)^{2/3} \frac{1}{r_s} \end{aligned} \tag{A.59}$$

where $r_s = \left(\frac{3}{4\pi\rho}\right)^{1/3}$ is the radius of a sphere that contains the charge of one electron [59, 60].

The correlation is a much more difficult problem than exchange, so exact analytic forms of $\epsilon_c^{LDA}(\rho)$ are known only for two limiting cases.

The first is the high-density (weak correlation) limit of a spin-compensated uniform electron gas [59, 60].

$$\epsilon_c^P(r_s) = A_{GB}\ell n(r_s) + B + r_s(C\ell n(r_s) + D)\ , \ \ r_s \ll 1\ . \tag{A.60}$$

The constant A_{GB} and B were evaluated by Gell-Mann and Brueckner [65], C and D by Carr and Maradudin [66]. Specifically,

$$A_{GB} = \frac{1 - \ell n2}{\pi^2} \approx 0.031091\ a.u. \tag{A.61}$$

The second case is the low-density (strong correlation) limit obtained by Nozieres and Pines [67] and Carr [68]

$$\epsilon_c^P(r_s) = \frac{1}{2}\left(\frac{U_0}{r_s} + \frac{U_1}{r_s^{3/2}} + \frac{U_2}{r_s^2} + \dots\right)\ , \ \ r_s \gg 1 \tag{A.62}$$

where U_k are again known constants. Similar formulas exist for $\epsilon_c^F(r_s)$ [59, 60].

The exact numerical values of $\epsilon_c^P(r_s)$ and $\epsilon_c^F(r_s)$ are known, with small statisti-

cal uncertainties for several intermediate values of r_s from Monte Carlo simulations of the uniform electron gas carried out by Ceperley and Alder [69]. Based on these results, several interpolation formulas for $\epsilon_c^P(r_s)$ and $\epsilon_c^F(r_s)$ have been devised to connect the high-density and low-density limits [Eqs.(A.60) and (A.62)] and simultaneously reproduce the Ceperley-Alder data for intermediate r_s.

A.2.6.2. Local Spin Density Approximation (LSDA)

In principle, the original Kohn-Sham formalism applies to both spin-compensated ($\rho_\alpha = \rho_\beta$) and spin-polarized ($\rho_\alpha \neq \rho_\beta$) systems. In spin-DFT, the basic variables are the spin-up and spin-down electron densities $\rho_\alpha(\boldsymbol{r})$ and $\rho_\beta(\boldsymbol{r})$ and also the exchange-correlation energy $E_{xc}[\rho_\alpha, \rho_\beta]$ is a functional of both [59, 60].

For uniform electron densities, $E_{xc}[\rho_\alpha, \rho_\beta]$ should reduce to the formulas for the exchange-correlation energy of a uniform free electron gas (the LSDA)

$$E_{xc}[\rho_\alpha, \rho_\beta] = E_{xc}^{LSDA}[\rho_\alpha, \rho_\beta] \quad \text{if } \rho_\sigma(\boldsymbol{r})\text{: constant.} \tag{A.63}$$

The extension of Eq.(A.58) to spin-polarized systems is called the local spin density approximation (LSDA). The LSDA exchange energy is

$$E_x^{LSDA}[\rho_\alpha, \rho_\beta] = -2^{1/3} C_x \int \left(\rho_\alpha^{4/3} + \rho_\beta^{4/3}\right) d\boldsymbol{r} \; . \tag{A.64}$$

Introducing the relative spin polarization

$$\xi = \frac{\rho_\alpha - \rho_\beta}{\rho_\alpha + \rho_\beta} \tag{A.65}$$

and using $\rho_\alpha = \frac{1}{2}(1+\xi)\rho$ and $\rho_\beta = \frac{1}{2}(1-\xi)\rho$ where $\rho = \rho_\alpha + \rho_\beta$, we rewrite Eq.(A.64) as

$$E_x^{LSDA}[\rho_\alpha, \rho_\beta] = \int \rho(\boldsymbol{r}) \epsilon_x(\rho, \xi) d\boldsymbol{r} \tag{A.66}$$

where

$$\epsilon_x(\rho, \xi) = -\frac{1}{2} C_x \rho^{1/3} \left[(1+\xi)^{4/3} + (1-\xi)^{4/3}\right] \; . \tag{A.67}$$

For a spin-compensated (paramagnetic : $\xi = 0$) electron gas,

$$\epsilon_x = \epsilon_x^P = -C_x \rho^{1/3} \tag{A.68}$$

and for fully-polarized (ferromagnetic : $\xi = \pm 1$)

$$\epsilon_x = \epsilon_x^F = -2^{1/3} C_x \rho^{1/3} \, . \tag{A.69}$$

For intermediate spin polarizations $0 < \xi < 1$, one can write $\epsilon_x(\rho, \xi)$ as an exact interpolation between the paramagnetic and ferromagnetic cases,

$$\epsilon_x(\rho, \xi) = \epsilon_x^P(\rho) + \left[\epsilon_x^F(\rho) - \epsilon_x^P(\rho)\right] f(\xi) \tag{A.70}$$

where the interpolating function is readily shown to be

$$f(\xi) = \frac{1}{2} \left[\frac{(1+\xi)^{4/3} + (1-\xi)^{4/3} - 2}{2^{1/3} - 1} \right] \, . \tag{A.71}$$

Even with accurate representations of $\epsilon_c^P(r_s)$ and $\epsilon_c^F(r_s)$ at our disposal, we need a general formula applicable to spin-polarized systems. Without loss of generality we can assume that, in analogy with Eq.(A.66),

$$E_c^{LSDA}[\rho_\alpha, \rho_\beta] = \int \rho(\boldsymbol{r}) \epsilon_c(r_s, \xi) d\boldsymbol{r} \tag{A.72}$$

where the function $\epsilon_c(r_s, \xi)$ is to be determined. Unfortunately, unlike for exchange, there is no simple exact formula relating $\epsilon_c(r_s, \xi)$ to $\epsilon_c^P(r_s)$, $\epsilon_c^F(r_s)$ and ξ. Von Barth and Hedin proposed using the same interpolating formula for $\epsilon_c(r_s, \xi)$ as for $\epsilon_x(\rho, \xi)$, that is,

$$\epsilon_c^{BH}(r_s, \xi) = \epsilon_c^P(r_s) + \left[\epsilon_c^F(r_s) - \epsilon_c^P(r_s)\right] f(\xi) \tag{A.73}$$

where $f(\xi)$ is given by Eq.(A.71). In practice, Eq.(A.73) is not very accurate. Vosko, Wilk

and Nusair [70] examined several alternatives to the Barth-Hedin interpolation formula and recommended the following expression

$$\epsilon_c^{VWN}(r_s,\xi) = \epsilon_c^P(r_s) + \alpha_c(r_s)\left[\frac{f(\xi)}{f''(0)}\right](1-\xi^4) + \left[\epsilon_c^F(r_s) - \epsilon_c^P(r_s)\right] f(\xi)\xi^4 \ , \quad \text{(A.74)}$$

where $\alpha_c(r_s)$ is a new function called spin stiffness. The spin stiffness is formally defined as

$$\alpha_c(r_s) = \left[\frac{\partial^2 \epsilon_c(r_s,\xi)}{\partial \xi^2}\right]_{\xi=0} \quad \text{(A.75)}$$

and fitted to the same analytic form as $\epsilon_c^P(r_s)$ and $\epsilon_c^F(r_s)$.

A.2.6.3. Generalized Gradient Approximation (GGA)

As soon as the extent of the approximations contained in the LDA has been understood, one can start constructing better approximation. This approximation is called the generalized gradient approximation (GGA) [71]. The GGA for exchange correlation energy improves on the LSDA description of atoms and molecules. The most popular approach is to specify semi-locally the inhomogeneities of the density, by expanding the exchange correlation energy $E_{xc}^{GGA}[\rho]$ as a series in terms of the electron density and its gradient as [41, 71, 72]

$$E_{xc}^{GGA}[\rho_\alpha,\rho_\beta] = \int d^3r \rho(\boldsymbol{r}) \epsilon_{xc}\left(\rho_\alpha(\boldsymbol{r}),\rho_\beta(\boldsymbol{r}),\nabla\rho_\alpha(\boldsymbol{r}),\nabla\rho_\beta(\boldsymbol{r})\right) \ . \quad \text{(A.76)}$$

A.2.6.4. Hybrid Functional (B3LYP)

A hybrid functional mixes together the formula for E_{xc} with the gradient-corrected E_x and E_c formulas [37]. For example, the popular B3LYP (Becke-three-LeeYangParr) hybrid functional (where 3 indicates a three parameter functional) is defined by

$$E_{xc}^{B3LYP} = (1-a-b)\, E_x^{LSDA} + a\, E_x^{exact} + b\, E_x^{B88} + (1-c)\, E_c^{VWN} + c\, E_c^{LYP} \quad \text{(A.77)}$$

where

$$E_x^{LSDA} = -\frac{3}{4}\left(\frac{6}{\pi}\right)^{1/3} \int \left[\left(\rho^{\alpha}\right)^{4/3} + \left(\rho^{\beta}\right)^{4/3}\right] d^3\boldsymbol{r} \; . \tag{A.78}$$

E_x^{exact} (which is sometimes denoted E_x^{HF}, since it uses a Hartree-Fock definition of E_x) is given by, E_x^{B88} is the Becke's 1988 gradient-corrected exchange functional [73]. E_c^{VWN} is the Vosko-Wilk-Nusair [70] expression for the LSDA correlation functional. Lastly, E_c^{LYP} is the Lee-Yang-Parr gradient-corrected correlation functional [74] and the parameter values $a = 0.20$, $b = 0.72$ and $c = 0.81$ were chosen to give good fits to experimental molecular atomization energies.

APPENDIX B

HARTREE-FOCK MEAN FIELD APPROXIMATION FOR THE MULTI-ORBITAL ANDERSON MODEL

B.1. Anderson Model

In Eq.(2.23), we have defined the Anderson model Hamiltonian $\mathcal{H}$ as

$$\begin{aligned}\mathcal{H} &= \sum_{m\sigma}(\varepsilon_m - \mu)c^{\dagger}_{m\sigma}c_{m\sigma} + \sum_{\nu\sigma}(\varepsilon_{d\nu} - \mu)d^{\dagger}_{\nu\sigma}d_{\nu\sigma} + \sum_{m\nu\sigma}\left(V_{\nu m}d^{\dagger}_{\nu\sigma}c_{m\sigma} + h.c.\right) + \\ &\quad + \sum_{\nu} U_{\nu}n_{\nu\uparrow}n_{\nu\downarrow} \\ &= H_0 + \sum_{\nu} U_{\nu}n_{\nu\uparrow}n_{\nu\downarrow}. \end{aligned} \tag{B.1}$$

In Eq.(B.1), U_ν is the value of the on-site Coulomb repulsion, $n_{\nu\sigma} = d^{\dagger}_{\nu\sigma}d_{\nu\sigma}$ is the occupancy of the $3d$ orbitals for spin $\sigma = (\uparrow$ or $\downarrow)$, and $d^{\dagger}_{\nu\sigma}$ and $d_{\nu\sigma}$ are the fermion creation and annihilation operators at the $3d$ orbitals.

The local electron densities at the $3d$ orbitals for spin-up and spin-down can be written as

$$n_{\nu\uparrow} = \frac{1}{2}(n_\nu + m_\nu)$$

$$n_{\nu\downarrow} = \frac{1}{2}(n_\nu - m_\nu) \tag{B.2}$$

so that the magnetization at each $3d$ orbital becomes

$$m_\nu = n_{\nu\uparrow} - n_{\nu\downarrow} \tag{B.3}$$

and the electron density is given by

$$n_\nu = n_{\nu\uparrow} + n_{\nu\downarrow}. \tag{B.4}$$

In the mean field approximation, the occupancy of the $3d$ orbitals is rewritten as

$$n_{\nu\uparrow} = \langle n_{\nu\uparrow}\rangle + (n_{\nu\uparrow} - \langle n_{\nu\uparrow}\rangle), \tag{B.5}$$

$$n_{\nu\downarrow} = \langle n_{\nu\downarrow}\rangle + (n_{\nu\downarrow} - \langle n_{\nu\downarrow}\rangle). \tag{B.6}$$

Here, we use approximation that $n_{\nu\sigma} - \langle n_{\nu\sigma}\rangle$ is much less than $n_{\nu\sigma}$. Hence, we use

$$\begin{aligned} n_{\nu\uparrow}n_{\nu\downarrow} = \langle n_{\nu\uparrow}\rangle\langle n_{\nu\downarrow}\rangle + \langle n_{\nu\uparrow}\rangle (n_{\nu\downarrow} - \langle n_{\nu\downarrow}\rangle) + \langle n_{\nu\downarrow}\rangle(n_{\nu\uparrow} - \langle n_{\nu\uparrow}\rangle) + \\ + (n_{\nu\uparrow} - \langle n_{\nu\uparrow}\rangle)(n_{\nu\downarrow} - \langle n_{\nu\downarrow}\rangle) \end{aligned} \tag{B.7}$$

where the last term is neglected due to it being very small. This way, we obtain

$$n_{\nu\uparrow}n_{\nu\downarrow} \cong n_{\nu\uparrow}\langle n_{\nu\downarrow}\rangle + n_{\nu\downarrow}\langle n_{\nu\uparrow}\rangle - \langle n_{\nu\uparrow}\rangle\langle n_{\nu\downarrow}\rangle \tag{B.8}$$

by using the mean-field approximation for the Anderson model. Thus, the mean-field Hamiltonian becomes

$$H_{MF} = H_0 + \sum_{\nu=1}^{5} [U_\nu\langle n_{\nu\downarrow}\rangle n_{\nu\downarrow} + U_\nu\langle n_{\nu\uparrow}\rangle n_{\nu\uparrow} - U_\nu\langle n_{\nu\uparrow}\rangle\langle n_{\nu\downarrow}\rangle] \tag{B.9}$$

where $n_{\nu\uparrow}$ ($n_{\nu\downarrow}$) is defined by $d^\dagger_{\nu\uparrow}d_{\nu\uparrow}$ ($d^\dagger_{\nu\downarrow}d_{\nu\downarrow}$). Consequently, the final form of the mean-

field Hamiltonian H_{MF} is given by

$$\begin{aligned} H_{MF} = & \sum_{m\sigma} (\varepsilon_m - \mu) c^\dagger_{m\sigma} c_{m\sigma} + \\ & + \sum_{\nu} \left[\left(\varepsilon_{d\nu} - \mu + U_\nu \langle n_{\nu\downarrow} \rangle \right) d^\dagger_{\nu\uparrow} d_{\nu\uparrow} + \left(\varepsilon_{d\nu} - \mu + U_\nu \langle n_{\nu\uparrow} \rangle \right) d^\dagger_{\nu\downarrow} d_{\nu\downarrow} \right] + \\ & + \sum_{m\nu\sigma} \left(V_{\nu m} d^\dagger_{\nu\sigma} c_{m\sigma} + h.c. \right) - \sum_{\nu} U_\nu \langle n_{\nu\uparrow} \rangle \langle n_{\nu\downarrow} \rangle . \end{aligned} \tag{B.10}$$

For H_0, we define the Green's functions as follows:

$$G^\sigma_{\nu\nu}(\tau) = -\langle T d_{\nu\sigma}(\tau) d^\dagger_{\nu\sigma}(0) \rangle, \tag{B.11}$$

$$G^{00}_{\nu\sigma}(i\omega_n) = \frac{1}{i\omega_n - (\varepsilon_{d\nu} - \mu)} \qquad \text{for} \quad U_\nu = 0 \text{ and } V_{\nu m} = 0, \tag{B.12}$$

$$G^{0}_{\nu\sigma}(i\omega_n) = \frac{1}{i\omega_n - (\varepsilon_{d\nu} - \mu) - F_{\nu 0}(i\omega_n)} \qquad \text{for} \quad U_\nu = 0 \text{ and } V_{\nu m} \neq 0 \tag{B.13}$$

where the self-energy $F_{\nu 0}(i\omega_n)$ is defined by

$$F_{\nu 0}(i\omega_n) = \sum_m \frac{|V_{\nu m}|^2}{i\omega_n - (\varepsilon_m - \mu)}. \tag{B.14}$$

In Eq.(B.14), ω_n is the Matsubara frequency as $\omega_n = (2n+1)\pi T$.

In addition, for H_{MF}, we define the Green's functions as follows:

$$G^0_{\nu\uparrow}(i\omega_n) = \frac{1}{i\omega_n - (\varepsilon_{d\nu} - \mu + U_\nu \langle n_{\nu\downarrow} \rangle)} \qquad \text{for spin up,} \tag{B.15}$$

$$G^0_{\nu\downarrow}(i\omega_n) = \frac{1}{i\omega_n - (\varepsilon_{d\nu} - \mu + U_\nu \langle n_{\nu\uparrow} \rangle)} \qquad \text{for spin down.} \tag{B.16}$$

B.2. Self-Consistent Solution

We have already defined the Green's function at the d-site as

$$G^{\sigma}_{\nu\nu}(\tau) = -\langle T d_{\nu\sigma}(\tau) d^{\dagger}_{\nu\sigma}(0)\rangle, \tag{B.17}$$

$$G^{\sigma}_{\nu\nu}(\tau) = T\sum_{i\omega_n} e^{-i\omega_n\tau} G^{\sigma}_{\nu\nu}(i\omega_n). \tag{B.18}$$

Now, we introduce the self-consistency condition for the Green's functions at each d-site:

$$G^{\sigma}_{\nu\nu}(\tau = 0^-) = \langle d^{\dagger}_{\nu\sigma} d_{\nu\sigma}\rangle = \langle n_{\nu\sigma}\rangle, \tag{B.19}$$

$$G^{\sigma}_{\nu\nu}(\tau = 0^-) = T\sum_{i\omega_n} e^{-i\omega_n 0^-} G^{\sigma}_{\nu\nu}(i\omega_n) = \langle n_{\nu\sigma}\rangle. \tag{B.20}$$

We need to solve Eq.(B.20) for $\langle n_{\nu\sigma}\rangle$. Hence, we have ten equations with ten unknowns ($\nu = 1, \ldots, 5$ for d orbitals and $\sigma = \uparrow, \downarrow$ for spin up and down), which are given by the following

$$\begin{aligned}
f^{\uparrow}_1(\{x_i\}) &= T\sum_{i\omega_n} e^{-i\omega_n 0^-} G^{\uparrow}_{11}(i\omega_n) - \langle n_{1\uparrow}\rangle = 0,\\
&\vdots\\
f^{\uparrow}_5(\{x_i\}) &= T\sum_{i\omega_n} e^{-i\omega_n 0^-} G^{\uparrow}_{55}(i\omega_n) - \langle n_{5\uparrow}\rangle = 0,
\end{aligned} \tag{B.21}$$

$$\begin{aligned}
f^{\downarrow}_1(\{x_i\}) &= T\sum_{i\omega_n} e^{-i\omega_n 0^-} G^{\downarrow}_{11}(i\omega_n) - \langle n_{1\downarrow}\rangle = 0,\\
&\vdots\\
f^{\downarrow}_5(\{x_i\}) &= T\sum_{i\omega_n} e^{-i\omega_n 0^-} G^{\downarrow}_{55}(i\omega_n) - \langle n_{5\downarrow}\rangle = 0.
\end{aligned} \tag{B.22}$$

Here, $\{x_i\}$ represents $\{\{\langle n_{\nu\sigma}\rangle\}, \mu\}$.

For the host orbitals, we define the Green's function

$$G^{\sigma}_{mm'}(\tau) = \langle T c_{m\sigma}(\tau) c^{\dagger}_{m'\sigma}(0)\rangle, \tag{B.23}$$

which can be obtained from the following Feynman-diagram. In Fig.(B.1), we express

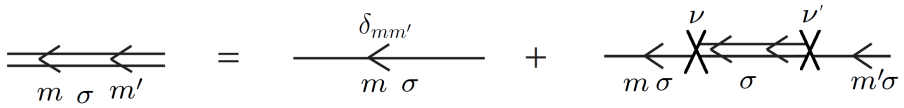

Figure B.1. Feynman diagram representing the host Green's function $G^{\sigma}_{mm'}$ for $\sigma =\uparrow ,\downarrow$. The double lines indicate $G^{\sigma}_{mm'}$ (defines the host Green's function) and $G^{\sigma}_{\nu\nu'}$ (defines the impurity Green's function) while the single lines denote G^{0}_{m} and $G^{0}_{m'}$ (define the host Green's functions for $U = 0$). Here, the cross terms indicate the hybridization matrix elements between host and impurity.

these Feynman diagrams in terms of the Green's functions at $T = 0$ as follows

$$iG^{\sigma}_{mm'} = iG^{0}_{m}\delta_{mm'} + iG^{0}_{m}(-iV_{\nu m})iG^{\sigma}_{\nu\nu'}(-iV_{\nu' m'})iG^{0}_{m'} \ . \tag{B.24}$$

At finite temperatures, we then have

$$\begin{aligned} G^{\sigma}_{mm}(i\omega_n) &= G^{0}_{m}(i\omega_n) + G^{0}_{m}(i\omega_n)V_{\nu m}V_{\nu' m}G^{\sigma}_{\nu\nu'}G^{0}_{m}(i\omega_n) \\ &= G^{0}_{m}(i\omega_n)\left[1 + \left(\sum_{\nu\nu'} V_{\nu m}V_{\nu' m}G^{\sigma}_{\nu\nu'}\right) G^{0}_{m}(i\omega_n)\right] . \end{aligned} \tag{B.25}$$

Here, $G^{0}_{m}(i\omega_n)$ is defined by

$$G^{0}_{m}(i\omega_n) = \frac{1}{i\omega_n - (\varepsilon_m - \mu)} \ . \tag{B.26}$$

For the impurity orbitals, we define the Green's function

$$G^{\sigma}_{\nu\nu'}(\tau) = -\langle T d_{\nu\sigma}(\tau) d^{\dagger}_{\nu'\sigma}(0)\rangle \tag{B.27}$$

which can be obtained from the following Feynman-diagram. In Fig.(B.2), we express

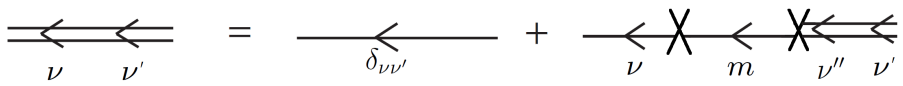

Figure B.2. Feynman diagram representing the impurity Green's function $G^{\sigma}_{\nu\nu'}$ for $\sigma =\uparrow,\downarrow$. The double lines indicate $G^{\sigma}_{\nu\nu'}$ and $G^{\sigma}_{\nu''\nu'}$ (define the impurity Green's functions) while the single lines denote G^{0}_{ν} and G^{0}_{m} (define respectively the impurity and host Green's function for $U = 0$). Here, the cross terms indicate the hybridization matrix elements between host and impurity.

these Feynman diagrams in terms of the Green's functions at $T = 0$ as follows

$$iG^{\sigma}_{\nu\nu'} = \delta_{\nu\nu'} iG^{0}_{\nu} + iG^{0}_{\nu}(-iV_{\nu m})(iG^{0}_{m})(-iV_{\nu'' m})iG^{\sigma}_{\nu''\nu'}, \tag{B.28}$$

$$\begin{aligned} G^{\sigma}_{\nu\nu'} &= \delta_{\nu\nu'} G^{0}_{\nu} + G^{0}_{\nu} \sum_{m} V_{\nu m} G^{0}_{m} \sum_{\nu''} V_{\nu'' m} G^{\sigma}_{\nu''\nu'} \\ &= \delta_{\nu\nu'} G^{0}_{\nu} + \sum_{\nu''} \left(G^{0}_{\nu} \sum_{m} V_{\nu m} G^{0}_{m} V_{\nu'' m} \right) G^{\sigma}_{\nu''\nu'}. \end{aligned} \tag{B.29}$$

From Eq.(B.29), we can write

$$G^{\sigma}_{\nu\nu'} = \delta_{\nu\nu'} G^{0}_{\nu} + \sum_{\nu''} W_{\nu\nu''} G^{\sigma}_{\nu''\nu'} \tag{B.30}$$

where $W_{\nu\nu''}$ is defined by

$$W_{\nu\nu''} = G^{0}_{\nu} \sum_{m} V_{\nu m} G^{0}_{m} V_{\nu'' m}. \tag{B.31}$$

From Eq.(B.30),

$$G^{\sigma}_{\nu\nu'} - \sum_{\nu''} W_{\nu\nu''} G^{\sigma}_{\nu''\nu'} = \delta_{\nu\nu'} G^{0}_{\nu}, \tag{B.32}$$

$$\sum_{\nu''} \left[\delta_{\nu\nu''} - W_{\nu\nu''}\right] G^{\sigma}_{\nu''\nu'} = \delta_{\nu\nu'} G^{0}_{\nu}$$

$$\sum_{\nu''} Z_{\nu\nu''} G^{\sigma}_{\nu''\nu'} = \delta_{\nu\nu'} G^{0}_{\nu} \tag{B.33}$$

and $Z_{\nu\nu''}$ is defined by

$$Z_{\nu\nu''} = \delta_{\nu\nu''} - W_{\nu\nu''}. \tag{B.34}$$

This equation is also valid for $T \neq 0$. Hence, we have

$$G^{\sigma}_{\nu\nu'}(i\omega_n) = \left(\sum_{\nu''} \left[\left(Z(i\omega_n) \right)^{-1} \right]_{\nu\nu''} \right) \left(\delta_{\nu''\nu'} G^{0}_{\nu''}(i\omega_n) \right)$$

$$G^{\sigma}_{\nu\nu'}(i\omega_n) = \left[\left(Z(i\omega_n) \right)^{-1} \right]_{\nu\nu'} G^{0}_{\nu'}(i\omega_n). \tag{B.35}$$

The last equation is obtained by setting the total number of electrons,

$$N_{el} = 718 = \sum_{m\sigma} \langle c^{\dagger}_{m\sigma} c_{m\sigma} \rangle + \sum_{\nu\sigma} \langle d^{\dagger}_{\nu\sigma} d_{\nu\sigma} \rangle \tag{B.36}$$

where $N_{el} = 718$ is the total number of electrons for the cyanocobalamin. This equation can be rewritten as

$$f_{11}(\{x_i\}) = \sum_{m\sigma} \langle c^{\dagger}_{m\sigma} c_{m\sigma} \rangle + \sum_{\nu\sigma} \langle d^{\dagger}_{\nu\sigma} d_{\nu\sigma} \rangle - 718 = 0. \tag{B.37}$$

Hence, there are 11 equations with 11 unknowns: $\langle n_{\nu\sigma} \rangle$'s and μ. We solve these equations by using the fortran program with LAPACK subroutines.

In Eq.(B.37), $\langle n_{\nu\sigma} \rangle = \langle d^{\dagger}_{\nu\sigma} d_{\nu\sigma} \rangle$ is obtained from Eq.(B.20)

$$\langle d^{\dagger}_{\nu\sigma} d_{\nu\sigma} \rangle = T \sum_{i\omega_n} e^{-i\omega_n 0^-} G^{\sigma}_{\nu\nu}(i\omega_n) \tag{B.38}$$

and $\langle n_{m\sigma} \rangle = \langle c^{\dagger}_{m\sigma} c_{m\sigma} \rangle$ is obtained from

$$\langle c^{\dagger}_{m\sigma} c_{m\sigma} \rangle = T \sum_{i\omega_n} e^{-i\omega_n 0^-} G^{\sigma}_{mm}(i\omega_n) \tag{B.39}$$

which is given in Eq.(B.25) with $G^{\sigma}_{\nu\nu'}(i\omega_n)$ substituted from Eq.(B.35). Thus, here,

$$G^{\sigma}_{mm}(i\omega_n) = G^{0}_{m}(i\omega_n) \left[1 + \left(\sum_{\nu\nu'} V_{\nu m} V_{\nu' m} \left[\left(Z(i\omega_n) \right)^{-1} \right]_{\nu\nu'} G^{0}_{\nu'}(i\omega_n) \right) G^{0}_{m}(i\omega_n) \right]. \tag{B.40}$$